## Title
Establishing Cerebral Organoids as Models of Human-Specific Brain Evolution.



## Journal
Cell, 176(4)

## ISSN
0092-8674

## Authors
Pollen, Alex A
Bhaduri, Aparna
Andrews, Madeline G
et al.

## Publication Date
2019-02-01

## DOI
10.1016/j.cell.2019.01.017

Peer reviewed

Published in final edited form as:

*Cell*. 2019 February 07; 176(4): 743–756.e17. doi:10.1016/j.cell.2019.01.017.

# Establishing Cerebral Organoids as Models of Human-Specific Brain Evolution

**Alex A. Pollen**[1,2,+,*,#], **Aparna Bhaduri**[1,2,*], **Madeline G. Andrews**[1,2], **Tomasz J. Nowakowski**[1,3], **Olivia S. Meyerson**[1,2], **Mohammed A. Mostajo-Radji**[1,2], **Elizabeth Di Lullo**[1,2], **Beatriz Alvarado**[1,2], **Melanie Bedolli**[1,2], **Max L. Dougherty**[4], **Ian T. Fiddes**[5], **Zev N. Kronenberg**[4], **Joe Shuga**[6], **Anne A. Leyrat**[6], **Jay A. West**[6], **Marina Bershteyn**[2], **Craig B. Lowe**[7], **Bryan J. Pavlovic**[1,2], **Sofie R. Salama**[5], **David Haussler**[5,8], **Evan E. Eichler**[4,8], and **Arnold R. Kriegstein**[1,2,#]

[1.]Department of Neurology, University of California, San Francisco (UCSF), San Francisco, CA, USA.

[2.]The Eli and Edythe Broad Center of Regeneration Medicine and Stem Cell Research, UCSF, San Francisco, CA, USA.

[3.]Department of Anatomy, UCSF, San Francisco, CA, USA.

[4.]Department of Genome Sciences, University of Washington School of Medicine, Seattle, WA, USA

[5.]Genomics Institute, University of California, Santa Cruz, CA, USA

[6.]New Technologies, Fluidigm, South San Francisco, CA, USA.

[7.]Department of Developmental Biology, Stanford University, Stanford CA, USA

[8.]Howard Hughes Medical Institute

## Summary:

Direct comparisons of human and non-human primate brains can reveal molecular pathways underlying remarkable specializations of the human brain. However, chimpanzee tissue is inaccessible during neocortical neurogenesis when differences in brain size first appear. To identify human-specific features of cortical development, we leveraged recent innovations that

[#]Correspondence should be addressed to: alex.pollen@ucsf.edu, arnold.kriegstein@ucsf.edu.

AUTHOR CONTRIBUTIONS

Methodology: AB, TJN, MGA, JS, AAL, JAW, CL, OSM, AAP. Investigation: AAP, AB, TJN, OSM, EDL, MAMR, BA, MaB, MeB, MGA. Resources: BP, MaB. Software: CBL, ITF. Formal analysis AB, TJN, MGA, ZNK, MLD, CBL, ITF, OSM, AAP. Writing: AAP, AB, with input from all authors. Funding acquisition ARK AAP. Conceptualization AAP. Supervision: ARK, SRS, DH, EEE, AAP.

[+]Lead contact: alex.pollen@ucsf.edu

[*]These authors contributed equally



DECLARATION OF INTERESTS

A.A.P. is a scientific advisor to System1 Biosciences. A.R.K. is a FR IRXQGHU DQG ERDUG PHPEHU RI 1HXURQD 7KHUDSHXWLFV.

permit generating pluripotent stem cell-derived cerebral organoids from chimpanzee. Despite metabolic differences, organoid models preserve gene regulatory networks related to primary cell types and developmental processes. We further identified 261 differentially-expressed genes in human compared to both chimpanzee organoids and macaque cortex, enriched for recent gene duplications, and including multiple regulators of PI3K/AKT/mTOR signaling. We observed increased activation of this pathway in human radial glia, dependent on two receptors up-regulated specifically in human, INSR and ITGB8. Our findings establish a platform for systematic analysis of molecular changes contributing to human brain development and evolution.

## Introduction:

The three-fold expansion of the human cerebral cortex is one of the most conspicuous features distinguishing humans from other great apes (Herculano-Houzel, 2012). This size difference is already apparent during early cortical development at mid-gestation, prior to the completion of neurogenesis (Sakai et al., 2012). Longstanding models propose that increased numbers of neural stem and progenitor cells could account for human brain expansion (Rakic, 1995). Radial glia act as neural stem cells to generate excitatory neurons of the cerebral cortex (Noctor et al., 2001), and recent comparative studies suggest a cell-intrinsic increase in proliferative divisions among radial glia as a candidate mechanism for human brain expansion (Otani et al., 2016). Nonetheless, the molecular basis for differences in developmental cell behavior remains poorly understood because primary brain tissue is largely inaccessible from chimpanzees, our closest living relatives, during developmental stages in which neurons of the cortex are generated.

Induced pluripotent stem cells (iPSCs) derived from great apes provide a platform for experimentally addressing how human-specific genetic changes differentially affect aspects of development (Blake et al., 2018; Gallego Romero et al., 2015; Marchetto et al., 2013; Pavlovic et al., 2018; Prescott et al., 2015; Silver, 2016). Organoid models derived from pluripotent stem cells harness natural properties of self-assembly to mimic early developmental processes across diverse tissues (Eiraku et al., 2008; Eiraku et al., 2011; Clevers, 2016). Recent studies have begun to compare gene expression between human and chimpanzee cerebral organoids from a limited number of individuals (Mora-Bermúdez et al., 2016), but systematic quantitative comparisons across multiple individuals and time-points are required to distinguish species differences from individual differences. Additionally, primate outgroups beyond chimpanzee are necessary to determine which evolutionary changes are derived in the human lineage. Similarly, analysis of the fidelity of organoid models to primary tissue requires comparing key sources of biological and technical variation across a range of protocols and individuals.

Single cell RNA sequencing provides an opportunity to compare gene expression in homologous cell types between primary tissue and organoid models and across species (Pollen et al., 2014; Camp et al., 2015). Although developing tissue and organoid models contain a diversity of cell types, new analysis methods allow for the identification of homologous cell types and gene regulatory networks based on the expression of thousands of genes in single cells (Butler et al., 2018; Nowakowski et al., 2017). Here, we use single

cell gene expression comparisons across the span of cortical neurogenesis to undertake three analyses that together enable the study of gene regulatory evolution during human brain development (Figure 1A). First, we examine the extent to which cell types, gene co-expression patterns, and developmental trajectories from primary tissue samples are preserved in organoid models. Second, we explore how gene expression patterns diverge between human and macaque during cortical development using primary tissue. Finally, we analyze which of the expression differences between human and macaque emerged along the human lineage in the last six million years using human and chimpanzee organoid models that give us an otherwise inaccessible window into patterns of early brain development in our closest living ancestor.

We find that organoid models preserve the vast majority of gene co-expression patterns observed in primary tissue during cortical development, supporting the utility of these models for studying the evolution of gene regulation. Nonetheless, across commonly used protocols, organoid models display a heterogeneous composition and upregulation of glycolysis, endoplasmic reticulum stress, and electron transport pathways, isolating potentially important differences with primary tissue, while also highlighting avenues for further improving this useful model. Similarly, we find striking conservation of gene networks across human, chimpanzee and macaque. However, we also identify a common set of 261 genes that are differentially expressed between human and macaque primary cortical cells and between human and chimpanzee organoid cells. These candidate human-specific gene expression differences are largely distinct from those reported in fibroblasts and pluripotent stem cells (Gallego Romero et al., 2015) and include many genes overlapping recent segmental duplications. Interestingly, we find increased activation of the PI3K/AKT/mTOR pathway specifically in human outer subventricular zone radial glia. Across species, radial glia are particularly sensitive to perturbations in this pathway compared with other cell types, and we show that pS6 activation in human depends in part on two genes, INSR and ITGB8, that are up-regulated in the human lineage, suggesting a molecular mechanism that may contribute to human-specific changes in neural stem cell behavior.

## Results:

### Cell diversity in primary samples and organoid models

Cortical development involves the emergence of diverse communities of cells, including excitatory neuron lineage cells (radial glia, intermediate progenitor cells, excitatory neurons), inhibitory neurons that migrate to the cortex from the ventral telencephalon, glial cells (astrocytes, oligodendrocytes, and microglia), and vascular cells. Organoid models may capture a subset of these cell types while also introducing additional sources of variation in cell types, cell states, and gene expression (Quadrato et al., 2017). We reasoned that single cell gene expression would allow us to evaluate the extent to which cell types, gene regulatory networks, and developmental trajectories are preserved in organoid models. Therefore, we designed a large-scale experiment to compare single cell gene expression using a standardized protocol across primary tissue from 48 human samples (Nowakowski et al., 2017) and 6 macaque samples with 56 organoids derived from 10 human and 8 chimpanzee individuals, distributed across stages of cortical neurogenesis (Figure 1B, Tables

S1–S2). We generated organoids based on a protocol developed in the Sasai lab (Kadoshima et al., 2013), and we further analyzed published single cell gene expression data from two other organoid protocols representing a continuum of guided to unguided patterning (Camp et al., 2015; Lancaster et al., 2013; Sloan et al., 2017) (Figure S1). To analyze the largest number of homologous genes across human, chimpanzee, and macaque, we updated gene models and orthology assignments in both chimpanzee and macaque genomes using the comparative annotation toolkit (Fiddes et al., 2018), providing a more accurate and comparable estimate of gene expression levels between species. In addition, we recently improved the contiguity of the chimpanzee genome through de novo assembly, increasing alignment rates (Kronenberg et al., 2018). Using these improvements, we were able to align reads to each species' native genome and examine gene expression across 49,360 orthologous genes (Figure S1). The number of genes detected per cell was comparable in human and chimpanzee organoids, but slightly lower in macaque, indicating that expression values may be underestimated for some macaque genes (Figure S1).

To characterize the cellular heterogeneity of organoid models, we first analyzed the frequency of cells expressing marker genes for cortical cell types as well as for common off-target lineages. The majority of human and chimpanzee organoids expressed markers of telencephalic regional identity, including cortical excitatory lineage cells, and a subset of inhibitory neurons from ventral telencephalon (Figures 1C, S1). A minority of organoids predominantly contained off-target lineages, including hindbrain, choroid plexus, retina, and mesenchymal cells, with a few individuals mainly accounting for the bias in differentiation potential (Figures S1, S2). For example iPS lines from two human individuals repeatedly produced off-target, largely hindbrain cells (8/9 organoids), while the other eight human individuals mainly produced telencephalon cells (18/22 organoids). Nonetheless, among telencephalon organoids, we observed additional variation in the proportion of excitatory and inhibitory neurons, indicating experimental variation in composition (Figure 1C). To further compare the cellular heterogeneity of primary cortical tissue and organoids, we performed immunohistochemistry for proteins that label radial glia and excitatory neurons. The human and macaque primary cortex samples displayed clear organization of radial glia and intermediate progenitors in the ventricular and subventricular zones and neurons migrating toward the cortical plate over an extensive intermediate zone. Similarly, cortical-like organoids from both human and chimpanzee contained ventricular and subventricular zone-like structures in which cells expressed markers of radial glia and intermediate progenitors (Fig. 1D). Outside of these zones, we observed cells expressing deep and upper layer markers at 6 and 15 weeks of organoid differentiation, respectively (Figures 1D, S1), but the overall distance from the ventricle to the periphery was greatly compressed compared to primary samples. Thus organoid models contained cell types and histological features reflective of cortical germinal zones, but demonstrated restricted structural organization and varied in composition across experiments.

We next sought to define homologous cell types across model systems and species. Although all cells were dissociated and captured using a common protocol, biological and technical differences across primary and organoid cells and between species create challenges for unbiased clustering of combined datasets (Figure S2). To overcome this limitation, we performed canonical correlation analysis (Butler et al., 2018), which finds

common sources of variation across datasets, to co-cluster cells from different model systems in three pairwise comparisons. For the organoid report card analysis, we co-clustered human primary and human organoid cells (Figure 2A). For the comparative analysis in primary tissue samples, we co-clustered human and macaque primary cells (Figure 2B), and for the comparative analysis in organoid samples, we co-clustered human and chimpanzee cells (Figure 2C). In each case, we identified major telencephalic cell types including radial glia across cell cycle phases, intermediate progenitor cells, excitatory neurons at different stages of maturation, and inhibitory neurons. These cell types were present across model systems and species and repeatedly emerged across individuals and with alternative co-clustering methods (Figures 2A–C, S2). In addition, most individuals contributed to most clusters, indicating that cell type and state drove clustering rather than individual or species (Figure S2). Interestingly, the overall cell composition was highly similar across species in both the primary sample comparison of human and macaque and the organoid comparison of human and chimpanzee. However, human primary samples and human organoids differed in composition, with primary telencephalon samples containing a greater proportion of interneurons, and organoids containing a greater proportion of radial glia and glycolytic cells (Figure S2). Together, these analyses provided a baseline for comparing cells of the same type across model systems and species.

## Preservation and conservation of gene co-expression patterns

Gene co-expression relationships often reflect biological processes related to cell type, cell state, and signaling pathways, in which many genes with related functions are coordinately regulated (Oldham et al., 2008; Langfelder & Horvath, 2008). To identify gene co-expression relationships, we performed weighted gene correlation network analysis (WGCNA) separately in each dataset (Figure 3A). Importantly, gene co-expression relationships can be determined independently from cell clustering results, providing an additional method for comparing datasets. We applied this approach to examine the extent to which gene co-expression modules are preserved between primary samples and organoid models and conserved across species by separately determining gene co-expression relationships in all primary human cells, all primary macaque cells, all human organoid cells, and all chimpanzee organoid cells (Tables S3–S4). Despite variation in cell composition, we found that the majority of co-expression modules derived independently in each dataset were highly correlated (Pearson's $R > 0.5$) (Figures 3A, S3). For example, over 70% of human primary modules showed a Pearson's correlation greater than 0.7 with a human organoid module. Overall, the shared patterns of co-expression provided systematic evidence for preserved gene regulatory mechanisms in organoid models and conservation of these regulatory relationships across species.

We next examined whether these co-expression modules related to common biological processes. Using a general linear model, we identified many modules related to cell type as independently defined by homologous clustering, but relatively few modules related to differences between individuals, between the organoid model system and primary samples, or between species (Figure S3). For example, many modules generated in each dataset correlated with radial glia and excitatory neuron clusters, while a subset correlated with intermediate progenitor and interneuron subtypes (Figure 3B). These relationships allowed

us to generate consensus modules related to cell type that emerge across all datasets (Figure 3C). Notably, individual modules related to finer aspects of cell subtype variation than could be discerned from the cell type clustering. For example modules correlated with radial glia cell identity included networks related to young radial glia (organoid.chimp.ME.lavenderblush3: *LIX1*, *HMGA2*), outer subventricular zone radial glia (primary.human.ME.palevioletred: *HOPX*, *SLCO1C1*, *MOXD1*, *S1PR1*), and mature radial glia (primary.human.ME.magenta: *CLU*, *ATP1A2*, *TNC* (Table S4). Similarly, modules correlated with inhibitory neurons included networks related to LGE- and CGE-derived (e.g., primary.human.ME.antiquewhite2: *PROX1*, *SCGN*, *CALB2*, *SP8*) and MGE-derived (primary.human.ME.yellow3: *MAF, LHX6, SST*) interneuron subtypes, with organoids enriched for LGE-derived interneuron subtypes (Figure S3). In addition, highly correlated modules that related to cell states independently emerged in all four datasets, including the G2/M and G1/S transitions and excitatory neuron maturation (Figure S3). On the other hand, modules related to cell types not commonly found in organoids, such as microglia, and oligodendrocyte precursors, emerged across species, but only in primary cell datasets (Figure S3). The independent emergence of modules highly correlated to cell type indicates that transcriptional programs determining cell types are largely conserved among primates and that gene regulatory mechanisms in major telencephalic cell types and states can be modeled in cerebral organoids.

## Developmental processes and metabolic states

We further examined the extent to which organoid models preserve developmental trajectories related to neuronal differentiation, radial glia maturation, and cortical areal identity that we recently described during normal cortical development (Nowakowski et al., 2017). As previously reported, the signature of differentiation from radial glia to excitatory neurons is highly correlated between primary cells and organoid models, with very few genes deviating from the *in vivo* trajectory (Figure 4A) (Camp et al., 2015). We similarly found that gene co-expression modules representing radial glia maturation independently arose in primary and organoid radial glia datasets (Figures 4B, S4). In addition, astrocyte production was restricted to the oldest organoid samples (Figure S4) as recently reported (Sloan et al., 2017). However, the radial glia maturation signature was more strongly correlated with primary sample age than with organoid age, indicating variability in the timing of organoid maturation (Figure 4B). The emergence of distinct cortical areas is a major feature of normal cortical development, and maturing excitatory neurons show transcriptional signatures of areal identity. Therefore, we used excitatory neurons from human primary visual (V1) and prefrontal cortex (PFC) to construct a classifier for the areal identity (Figure 4C). Consistent with previous immunohistochemical observations of gradients in several regional identity genes (Eiraku et al., 2008; Kadoshima et al., 2013), most organoids contained a mixture of V1-like and PFC-like excitatory neurons and additional neurons of unknown areal identity (Figure 4C). Overall, neuronal differentiation, radial glia maturation, and aspects of cortical arealization occurred spontaneously in organoid models, but the timing of radial glia maturation and arealization of neuronal identity was heterogeneous.

We next explored the biological processes that were strongly associated with organoid models when compared to primary cells. We hypothesized that differences resulting from the organoid system might be reflected across a range of cerebral organoid protocols and might illuminate general opportunities for improving these culture systems. Indeed, we found that three independent organoid protocols varying in their use of patterning molecules to constrain regionalization displayed upregulation for the same gene co-expression modules compared with primary samples (Figure 4D, S4). In particular, the modules with strongest organoid enrichment across protocols related to glycolysis (Figures 4D, S4). Interestingly, similar glycolysis gene co-expression modules emerged in primary human and primary macaque cells, but the expression of genes in these modules was higher and more pervasive in organoid cells (Figure 4E), indicating over-activation of a normal metabolic pathway. In addition, we observed enrichment in organoids for modules involving endoplasmic reticulum stress, including the unfolded protein response pathway and electron transport (Figures 4E, S5). In contrast, modules enriched in primary samples related to telencephalon regional identity and excitatory neuron subtypes that were also commonly observed in organoids but were found at a higher frequency in primary samples (Figure 4D). Overall, current organoid models preserve gene co-expression networks and developmental trajectories observed in primary tissue, while our analysis highlights specific targets for optimization of future organoid culture systems, including up-regulated metabolic stress pathways, impoverished cortical architecture, and the variability of cell composition across differentiation experiments (Figure S4).

## Human-specific gene expression changes

The preservation of gene regulatory networks and developmental processes in organoid models allowed us to search for gene expression patterns that evolved in the last six million years. Our strategy involved first comparing primary human and primary macaque cortex to identify gene expression differences that occur during normal development across more distant primates. Next, to identify which of these changes occurred in recent evolution, we compared gene expression in human and chimpanzee organoid models. We used a likelihood ratio test (LRT) commonly applied to single cell gene expression data and a general linear model to calculate differential expression, accounting for a large number of technical and biological replicates (Methods, Table S5). Across cells from primary telencephalon samples, we observed 1258 differentially-expressed genes between human and macaque, and across cells from organoids with a telencephalon identity, we observed 738 differentially-expressed genes between human and chimpanzee (Figure 5A, S6). The fold change and direction of these differentially expressed genes was correlated (Figure 5B–C) and 261 genes overlapped across comparisons ($P < 10^{-16}$), providing a set of candidate genes independently supported by primary tissue and organoid comparisons that are likely to have derived human-specific gene expression patterns during cortical development.

We further examined the properties of derived genes with respect to the specificity of differential expression and the overlap with genes underlying neurodevelopmental disorders. To examine the specificity of gene expression changes, we compared our results in developing cortex with recent studies in human and chimpanzee fibroblasts and iPS cells (Gallego Romero et al., 2015). Of the 261 candidate derived gene expression changes, 85%

were specific to cortical development (Figure 5D, S5). Nonetheless, these differences were frequently shared across cortical cell types (Figure 5E, S5). Because genes linked to autism spectrum disorder also show enriched expression in the stages and cell types of cortical development that we surveyed genes. Of 78 genes with an excess of (Bakken et al., 2016), we examined whether derived regulatory changes included disease-linked *de novo* mutations in autism (Stessman et al., 2017), five overlapped with the stringent set of 261 derived changes on the human lineage, and an additional four overlapped with a broader set of 668 genes differentially expressed in at least one cortical cell type (Figure 5E), including *SRCAP*, which also showed broad species differences by in situ hybridization (Figure S5). These overlaps were both moderately significant against the background set of all detected genes (hypergeometric $P < 0.005$.) Thus, our approach of combining primary sample and organoid comparisons revealed many candidate tissue-specific gene expression patterns during human brain development, and highlighted examples of disease-related genes that may have human-specific developmental functions.

Recent studies have identified human-specific genetic changes likely to influence gene regulation or gene copy number (Dennis et al., 2012; McLean et al., 2011; Pollard et al., 2006; Charrier et al., 2012; Dennis et al., 2017). By overlapping major classes of structural genomic changes with human-specific gene expression differences, we sought to identify candidate sequence changes particularly likely to influence gene expression during cortical development. We found that recently duplicated genes (Sudmant et al., 2013) were significantly over-represented among differentially-expressed genes (Figure 5F, $P < 10^{-7}$). For example, nearly all genes in the *SMN1* and *ARL17A* loci showed increased expression in human developing cortex compared to chimpanzee and macaque (Figure S5). This is perhaps unsurprising as the human genome contains additional copies of these duplicated genes. Nonetheless, human-specific duplications may also result in daughter genes with new expression patterns (Dennis et al., 2017). For example, the NPIP family, that has expanded in copy number in the ape and human lineage (Johnson et al., 2001), but only a single human paralog, *NPIPB5*, shows derived regulatory changes in cortical tissue (Table S6). Duplications that occurred earlier in ape evolution may also provide a substrate for additional regulatory changes (Dennis et al., 2017; Ohno, 1970). Therefore, we examined whether duplications that occurred in the human lineage prior to our divergence from chimpanzee were also enriched among derived regulatory changes. Overall, we found a modest enrichment for differential expression among these older duplication events ($P < 0.005$). These include intriguing examples, such as the monoamine transporter *SLC29A4*, which appears to have duplicated in the common ancestor of human and chimpanzee, but is more highly expressed in human cortical development, particularly in a subset of intermediate zone and cortical plate cells (Figures 5F, S5).

Models of regulatory evolution suggest that genetic changes influencing hub genes may increase the expression of species-specific regulatory networks. To identify gene networks that changed together in the human lineage through the influence of common regulatory mechanisms, we further analyzed whether gene co-expression modules showed human-specific expression patterns. We found that many co-expression modules enriched in primary human compared with primary macaque samples were also up-regulated in human organoid compared with chimpanzee organoid samples, suggesting human-specific regulation of these

networks (Figure 5G). The two strongest modules with a derived gain of expression in the human lineage were enriched for negative regulation of transcription related to G1/S transition and neuronal apoptosis ($P < 10^{-6}$). In addition, several modules with derived expression changes along the human lineage also showed enrichment for particular cell types (Table S4). These modules with species and cell type enrichment included primary.human.ME.darkred, whose upregulation in human radial glia may be partly driven by duplication of NBPF genes, and organoid.human.ME.skyblue4 that was downregulated in human excitatory neurons and contained genes related to axonal fasciculation. Together, these results provide candidate regulatory networks that may have evolved together through coordinated transcriptional changes.

Radial glia are particularly likely to influence the evolutionary expansion of the brain (Noctor et al., 2001; Rakic, 2003), and we next examined whether differentially-expressed pathways might influence radial glial development. We did not observe significant gene ontology enrichment among differentially expressed genes after multiple hypothesis correction, but genes in the PI3K/AKT/mTOR pathway appeared in the top-ranked categories (e.g., FOXO3 signaling p=0.065, Figures 6A, S6, Table S6). Further analysis of mTOR pathway genes revealed that both activators (INSR, ITGB8, IFNAR1) and repressors (PTEN) showed strong up-regulation in human organoids and human primary cells. Although this pathway is known to influence neuronal maturation, we recently observed strong immunoreactivity for the mTOR effector phosphorylated ribosomal S6 (pS6) in outersubventricular zone radial glia (Nowakowski et al., 2017). To determine whether patterns of mTOR activation changed in radial glia during recent human evolution, we first performed immunohistochemistry for pS6 across species using an antibody to conserved phosphorylation sites. We observed comparable levels of immunoreactivity among neurons in human and macaque cortical plate (Figure S6). However, in germinal zones, we found that pS6 strongly labeled human primary and organoid radial glial cells, in particular those away from the ventricle and ventricular zone-like regions (Figures 6B–C, S6). Conversely, staining in primary macaque and chimpanzee organoid sections showed less pervasive and fainter pS6 immunoreactivity than in human radial glia (Figures 6B–C, S6), suggesting that changes in the activity of the mTOR signaling pathway have evolved recently in human outer radial glia.

We next sought to further quantify changes in mTOR activation across species. Because many components of this pathway undergo post-translational regulation, we performed Western blots for INSR and the phosphorylated mTOR effectors S6, 4EBP1, and NRDG1. To enrich for progenitor cells, we cultured primary human and macaque cells for several passages in media that favors progenitors (Onorati et al., 2016) and we examined 5-week-old organoids that contain a high proportion of progenitors. We found that the candidate upstream factor INSR was upregulated at the protein level commensurate with expression differences determined by single cell RNA sequencing (Figure S6). In addition, pS6, p4EBP1, and pNRDG1 all showed increased abundance in human cells compared with chimpanzee organoid and primary macaque cells, consistent with up-regulation of the mTOR pathway in human. Because a subset of radial glia were pS6 positive in the non-human primate samples, we hypothesized that primate radial glia have the capacity to further activate the mTOR pathway in the presence of upstream factors. We therefore treated

primary macaque cells in monolayer and organotypic culture with BDNF and the MTOR activator 3-Benzyl-5-((2-nitrophenoxy)methyl)-dihydrofuran-2(3H)-one (3BDO) (Peng et al., 2014). Both activators led to increased pS6 levels in progenitors (Figure S6). This finding suggests that across primates, cortical progenitors are responsive to the mTOR pathway, but that human radial glia show a higher level of activation (Figure S6). To further probe for candidate upstream regulators explaining the increased activation in human progenitors, we examined whether INSR and ITGB8, two receptors upregulated in human, were necessary for normal pS6 activation in organotypic slice culture of primary human samples. We infected slices with shRNA lentiviral vectors targeting each gene and found that reducing INSR and ITGB reduced overall levels of pS6 (Figure 6C). Together, these results provide a candidate molecular mechanism governing human-specific changes in cortical radial glia signaling pathways.

## Discussion

Over the last six million years, genetic changes along the human lineage have driven remarkable changes in human brain structure, cognition, and behavior. These genetic changes likely influenced patterns of brain development because brain size differences appear *in utero*, and nearly all cortical neurons are generated prior to birth (Sakai et al., 2012). Thus, comparative studies of brain development are essential for understanding the molecular basis of human brain evolution. Genetic changes are particularly likely to influence gene expression, either directly through copy number or *cis*-regulatory changes or indirectly through the *trans*-regulatory effects of genes harboring mutations. However, in contrast to adult samples, prenatal brain tissue from chimpanzee, our closest living relative, is largely inaccessible to analyses of gene expression. Here, we sought to establish great ape cerebral organoids as a model system for studying human-specific molecular changes that influence neurogenesis. We found that gene regulatory mechanisms observed during neurogenesis in primary cortex are mostly recapitulated in organoid models, and we identified human-specific gene expression patterns during cortical neurogenesis through independent comparisons of human and primate primary cells and organoid models.

Because cerebral organoids are a relatively new model system, we developed a multi-dimensional report card of the correspondence between human cerebral organoids and primary tissue. Our findings indicate that organoid cell composition can vary across experiments, individuals, and protocols, but that underlying cell types, gene co-expression relationships, and developmental trajectories are preserved in organoid models across individuals, species, and protocols. The pathways distinguishing organoids - glycolysis, endoplasmic reticulum stress, and electron transport - provide useful targets for further optimization of cerebral organoid media and perfusion conditions and may also have implications for organoid studies of neurodegenerative disorders in which cellular stress pathways are known to accelerate the appearance of disease phenotypes. Together, our report card reveals the fidelity and robustness of developmental programs that can be modeled using cerebral organoids, and serves as a data-driven framework for evaluating organoid cells along biological axes of variation related to cell heterogeneity, neuronal differentiation, radial glia maturation, cortical arealization, and metabolic states. From the report card analysis, we concluded that comparative investigation of organoid models across species

provides a realistic window into gene regulatory changes in cortical evolution, but that independent analysis of primary cells from different species still provides crucial validation data independent from organoid models for determining species-specific gene expression patterns. Future improvements to organoid protocols that demonstrate reproducibility of cell composition and neuronal connectivity relationships may enable evolutionary analysis of addition facets of human and great ape brain development beyond this initial focus on gene regulation.

Human-specific genetic changes may affect cortical development by influencing gene regulatory networks active during neurogenesis. Although there is great interest in modeling the impact of human-specific genetic changes on brain development (Boyd et al., 2015; McLean, 2011; Pollard et al., 2006; Charrier et al., 2012; Dennis et al., 2012; Florio et al., 2016) a description of actual molecular differences during normal development is crucial for interpreting the consequences of genome sequence changes. Against a background of highly conserved gene expression patterns, we identify 261 candidate genes with derived expression changes in the human lineage. A subset of these changes are concerted across non-neural cell types, but the majority appear to be specific to developing cortex and shared across cortical cell types. These results are consistent with a hierarchical model in which regulatory mutations have different levels of pleiotropy from organism to tissue to cell type (Liang et al., 2018). In addition to individual genes, we identified several gene co-expression modules with increased expression along the human lineage, including modules enriched for genes affecting transcription during the G1/S transition and neuronal apoptosis, two developmental processes that may influence the number of progenitors and neurons. Future analysis of hub genes and candidate upstream factors in these networks may illuminate the causative genetic changes underlying gene expression differences. In addition, the recent de novo assembly of the chimpanzee genome and improved gene models enabled more accurate measurements of gene expression as a result of higher alignment rates to the native genome of each species (Kronenberg et al., 2018, Fiddes et al., 2018). Nonetheless, the annotation of gene models and expression levels of some genes may still be biased toward the higher quality human genome assembly, in particular with respect to macaque. Therefore, future improvements of gene annotations and genome assembly through long read sequencing in other primates will further strengthen comparative analyses. In addition, increased cellular coverage through droplet capture of single cells across many individuals and stages will make analysis more comprehensive, illuminating the most divergent gene networks, cell types, and developmental trajectories.

Several influential models suggest that human brain expansion may result from an increase in the number of radial glia early in development (Rakic, 2003), an increase in the number of outer subventricular zone progenitors (Fish et al., 2008; Kriegstein et al., 2006; Smart et al., 2002), and an extended neurogenic window (Rakic, 1995). In each of these models, signaling pathways controlling radial glia expansion and self-renewal represent candidate molecular pathways that could explain changes in developmental cell behavior. We recently observed increased activation of the LIFR/STAT3 self-renewal pathway in outer subventricular zone radial glia compared to ventricular radial glia that could support selective expansion of this secondary proliferative population during cortical development. However, this molecular signature was conserved in macaque radial glia and not likely

related to more recent human brain evolution (Pollen et al., 2015). Here, our comparative transcriptomic data among primates allowed us to examine additional signaling pathways that may have changed in more recent evolution. We find evidence that an increase in the activity of another key signaling pathway, PI3K/AKT/mTOR, distinguishes human outer subventricular zone radial glia from those in other primates. In many stem cell contexts, the mTOR pathway has been shown to promote stemness and long-term self-renewal (Zhou et al., 2009; Rafalski & Brunet, 2011). While it is possible that the increased levels of mTOR activation could be a consequence of increased proliferation in human radial glia, our results indicate that radial glia across primates are poised to activate mTOR signaling and suggest that increased levels of INSR and ITGB8 in human may contribute to recent evolutionary changes in pathway activation. Importantly, mTOR pathway mutations are associated with several human disorders, including autism, focal cortical dysplasia, and glioblastoma multiforme (Poduri et al., 2012; Ceccarelli et al., 2016). Our results suggest that during development, human outer subventricular zone radial glia may be particularly sensitive to perturbations in this pathway, and future studies may more directly assess the role of this pathway in human and primate neurogenesis. Together with recent work, our study adds to a burgeoning field of “cellular anthropology” (Prescott et al., 2015) by providing a comparative organoid platform for more systematically characterizing the specialized molecular features of human cortical development and evolution.

## STAR METHODS

### CONTACT FOR REAGENT AND RESOURCE SHARING

“Further information and requests for resources and reagents should be directed to and will be fulfilled by the Lead Contact, Alex A Pollen (Alex.Pollen@ucsf.edu).”

### EXPERIMENTAL MODEL AND SUBJECT DETAILS

**Cell lines and Samples—**We used previously described human and chimpanzee iPSC lines (Bershteyn et al., 2017; Gallego Romero et al., 2015; Pavlovic et al., 2018), and generated four additional lines from three chimpanzees (Table S1). All new lines were reprogrammed from fibroblasts using episomal plasmids according to a recently published protocol (Okita et al., 2013) and matching the protocol used for the majority of existing human and chimpanzee lines used in this study (Table S1). Low passage fibroblasts (P3 – P7) were obtained from the Coriell Cell Repository (Pt1: 12 year old chimpanzee male, catalog: PR00226; Pt2: 6 year old chimpanzee male, Maverick, catalog: S003611; Pt5: 8 year old chimpanzee male, catalog PR00738). For each line, we electroporated 300,000 fibroblasts with three micrograms of an episomal expression plasmid mixture encoding OCT3/4, SOX2, KLF4, L-MYC, LIN28, and shRNA for TP53 using a Neon Electroporator (Thermo Fisher), and a 100 μL kit, with setting of 1,650V, 10ms, and three pulses, as previously described (Bershteyn et al., 2017). After 5 – 8 days, electroporated cells were detached and seeded onto irradiated SNL feeder cells. Culture medium was replaced the next day with primate ESC medium (Reprocell) containing 5 – 20 ng/mL of βFGF, with higher levels of FGF producing better results. After 20 – 30 days, colonies were picked and selected for further cultivation. After three to five passages, colonies were transferred to Matrigel-coated dishes and maintained in mTeSR1 medium (Stem Cell Technologies, 05850)

supplemented with Penicillin/Streptomycin/Gentomycin. Further passaging was performed using calcium and magnesium free PBS to gently disrupt colonies. Each line showed a normal karyotype between passage 10 and 15. Macaque cortical tissue was generously provided from samples being used for other experiments from the UC Davis Primate Center. De-identified tissue samples were collected with previous patient consent in strict observance of the legal and institutional ethical regulations. Protocols, cell lines and samples were approved by UCSF GESCR (Gamete, Embryo, and Stem Cell Research) Committee.

**Organoid Differentiation Protocol—**We generated cerebral organoids according to previously published protocols (Kadoshima et al., 2013); (Bershteyn et al., 2017). Human and chimpanzee iPSCs were dissociated to single cells with Accutase and re-aggregated in lipidure-coated 96-well V-bottom plates at a density of 10,000 cells per aggregate, in 100 μL of cortical differentiation medium per well. The cortical differentiation medium (Glasgow-MEM, 20% KSR, 0.1mM NEAA, 1mM sodium pyruvate, 0.1mM β-ME, 100 U/mL penicillin/streptomycin) was supplemented with Rho Kinase Inhibitor (Y-27632, 20 μM, Tocris, Cat# 1254 day 0 and day 3), WNT inhibitor (IWR1-ε, 3 μM, Cayman Chemical Cat# 13659 days 0–18) and TGF-β inhibitor (SB431542, Tocris, Cat #1614, 5 μM, days 0–18). Media was changed on days 3 and 6 and then every 2–3 days until day 18. Aggregates were then transferred to ultra low adhesion 6-well plates in DMEM/F12 medium with Glutamax supplemented with N2, Lipid Concentrate, Fungizone (2.5 μg/mL), and penicillin/streptomycin (100 U/mL) and grown under 40% O2 5% CO2 conditions. After five weeks, FBS (10% v/v), Matrigel (1% v/v) and heparin (5 μg/mL) were added to the medium, and after 8 weeks organoids were transferred to lumox dishes (Sarstedt), which have a gas permeable base.

## METHOD DETAILS

**Immunohistochemistry—**Organoids were fixed using 4% paraformaldehyde (PFA) in PBS for 20 min. Primary samples were fixed in 4% PFA prepared in calcium and magnesium free phosphate buffered saline (PBS) (pH~10) overnight at 4°C wi th constant agitation. After fixation, organoids and primary tissue samples were washed in PBS (pH7.4), equilibrated in 30% sucrose in PBS overnight at 4°C, embedded in blocks with a 1:1 mixture of 30% sucrose/OCT compound (Tissue-Tek, VWR) and frozen at −80°C. Blocks were sectioned to a thickness of 16 −20 μm cryosections, and antigen retrieval was performed, by heating sections to 95° in 10mM sodium citrate (pH=6.0) for 15 min. Sections were then permeabilized and blocked with 10% donkey serum in PBS in 2% Triton X-100, 0.2% gelatin. Primary antibody incubations were performed at 4°C overnight and secondary incubations were performed at room temperature for 1–3 hr, followed by three 20 min washes in PBS, and staining with AlexaFluor secondary antibodies (Thermo Fisher, 1:1000 dilution). Primary antibodies included: sheep anti-TBR2 (EOMES, 1:150, R&D AF6166), rabbit anti-pS6 (1:100, Cell Signaling 2211S), goat anti-SOX2 (1:200, Santa Cruz SC17320), mouse anti-SOX2 (1:200, Santa Cruz SC365964), Mouse anti-TUJ1 (β III TUBULIN, Covance, MMS-435, 1:500), rabbit anti-PAX6 (Covance, PRB-278P, 1:500), rat anti-CTIP2 (BCL11B, 1:500, Abcam ab18465), rabbit anti-TBR1 (1:500, Abcam ab31940), rabbit anti-SATB2 (1:1000, Abcam ab34735).

**Single cell RNA sequencing—**For single cell dissociation, primary and organoid samples were cut into small pieces, and incubated with a pre-warmed solution of Papain (Worthington Biochemical Corporation) prepared according to manufacturer's instructions for 10 min at 37°C. After approximatel y 30 – 60 min incubation, samples were triturated and macaque samples older than E100 and organoids older than 14 weeks were spun through an ovomucoid gradient to remove debris. Cells were then pelleted at 300g and resuspended in PBS supplemented with 3% fetal bovine serum (Millipore Sigma). Samples were diluted to approximately 170,000 cells per ml before processing capture using Fluidigm C1 auto-prep system as previously described (Nowakowski et al., 2017; Pollen et al., 2014; 2015). We performed library preparation using the Illumina Nextera XT library preparation kit, and quantification using the Bioanalyzer (Agilent) according to manufacturer's protocols. Paired-end 100 bp sequencing was performed on the Illumina HiSeq2500.

**In Situ Hybridization—**Macaque (E64, 67, 80) and human (GW 13, 17, 19) tissue was fixed in 4% PFA in PBS overnight at 4°C wit h constant agitation and then embedded in a 50% O.C.T. (Sakura Finetek, 4583), 30% sucrose mix and frozen at −80°C. Tissue was cryosectioned at 16um thickne ss onto glass slides, post-fixed and hybridized for one hour at 70°C. Hybridization buffer contains 50% for mamide, 5× SSC buffer, 5× Denhart's solution (Thermo Fisher, 750018), 500ug/ml fish sperm DNA (Sigma, 11467140001) and 250ug/ml yeast RNA (Sigma, 10109223001). Hybridized tissue was incubated overnight at 70°C with riboprobes designed against a conserved region of the macaque and human transcripts for each gene of interest (See Key Resources Table). Probes were made using a T7 Megascript kit (Invitrogen, AM1334) with DIG RNA labeling mix (Roche, 11277073910). Tissue was washed and incubated with an anti-DIG antibody (Roche, 1109327491) for 80 minutes at room temperature. Sections were developed using a NBT/BCIP (Roche, 11681451001) solution for 12–72 hours until a sufficient intensity. Slides treated with the same probe were incubated for the same duration of time. Slides were stopped by three PBS washes, coverslipped using Prolong Gold (Thermo Fisher P36930) and dried overnight. Tissue sections were imaged using a Keyence BZ-X fluorescent microscope.

**Primary Dissociated Samples—**Culture dishes were prepared by overnight coating with 0.01% poly-L-ornithine (Millipore Sigma) at 37°C. After three water washes, plates were coated with 5 ug/ml laminin (Thermo Fisher) and 1 ug/ml fibronectin (Corning) for at least two hours. Following dissociation, cells were cultured as previously reported (Onorati et al., 2016). Unless otherwise indicated, the media contained N2 Supplement (1:100, Gibco), B27 supplement (1:1000, BDNF (5 ng/ml, R&D Systems Inc), Rock Inhibitor Y-27632 (10 uM, Stemgent), Penicillin/Streptomycin (100 Thermo Fisher), FGF-2 (20 ng/ml, Gibco), EGF (20 ng/ml, Gibco), Human Insulin (20 ug/ml, Millipore Sigma), U/ml) in DMEM/F12+GlutamaxTM-I (Gibco). Media was replaced every 3 days and cells were passaged were passaged when cultures reached ~80% confluency (approximately every 5–7 days).

For mTOR experiments, cultures were depleted of BDNF from culture media for four days prior to being treated with either DMSO (1:500), 250nM Rapamycin (Abcam, ab146591), 20ng/mL BDNF (Millipore Sigma, srp3014–10) or 6uM 3BDO (Millipore Sigma,

SML1687) for five days. A cmv::gfp adenovirus (1: 2,000, Vector biolabs, 1060) was added to the culture 24 hours prior to collection to detect morphological changes. Dissociated cells were fixed in the culture dish with 4% PFA in PBS for 45mins at 4°C. Cells were permeabilized and bloc ked with 10% donkey serum in PBS in 0.1% Triton X-100, 0.2% gelatin for 30 minutes. Primary antibodies were incubated at 4°C overnight, washed three times with PBS containing 0.1% Triton for 5 minutes and secondary antibodies incubated at room temperature for two hours. Antibodies included: goat anti-gfp (1:500, Abcam Ab5450), rabbit anti-pS6 (1:500, Cell Signaling 2211S) and mouse anti-SOX2 (1:200, Santa Cruz SC365964) and AlexaFluor secondary antibodies (Invitrogen, 1:1000 dilution). Dissociated cultures were imaged using a Keyence BZ-X fluorescent microscope.

**Primary Organotypic Slice Cultures—**Primary human (GW17–18) and macaque (E80) tissue was live sectioned with a vibratome at a thickness of 300uM. Slices were infected with cmv::gfp adenovirus (1: 2,000, Vector biolabs, 1060) for 30 minutes at 37°C and then plated on Millicell inserts (Millipore, PICM03050) in media containing 60% Basal Medium Eagle (BME) (Thermo Fisher 21010046), 25% Hank's BSS (UCSF cell culture facility CCFAJ001–171602), 10% FBS (Thermo Fisher, 16000044), 1% penicillin, streptomycin and glutamine (Thermo Fisher 10378016), 1% N-2 (Thermo Fisher, 17502048), and 0.66% d-(+)-glucose. One day after collection slices were infected with shRNA-containing lentivirus (Sigma TRCN0000000381 [shINSR] and Sigma TRCN0000413303 [shITGB8]) for 24 hours. After virus removal, the slices were cultured for an additional 4 days. Slices were fixed in 4% PFA in PBS for 1 hour at room temperature and washed with PBS overnight at 4°C. Antigen retrieval was perform ed on slices using 10× Citrate Buffer (Sigma, C9999**)** by incubating slices in solution heated to 90°C fo r 20 minutes. Slices were washed with PBS prior to being permeabilized and blocked with 10% donkey serum in PBS containing 0.1% Triton X-100 and 0.2% gelatin for 30 minutes. Slices were incubated with primary antibodies for 48 hours at 4°C, then washed three t imes with PBS with 0.1% Triton for a total of three hours. Slices were incubated in secondary antibodies at 4°C overnight. Primary antibodies used were goat anti-gfp (1:500, Abcam Ab5450), rabbit anti-pS6 (1:500, Cell Signaling 2211S), mouse anti-SOX2 (1:250, Santa Cruz SC365964) and rat anti-CTIP2 (BCL11B, 1:500, Abcam ab18465) and AlexaFluor secondary antibodies (Invitrogen, 1:500 dilution). Slices were imaged using a Leica sp5 X confocal microscope, and quantification was performed on pS6-labeled cells and DAPI labeled cells, as DAPI showed the most consistent labeling across slices.

**Alignments and gene models—**Trim Galore 3.7 was used to trim 20 bp of adaptor sequence, and paired-end alignments were performed using HISAT2 to the human reference genome GRCh38, the updated chimpanzee reference genome panTro6 (Kronenberg et al., 2018) or the macaque reference genome, rheMac8. For each cell, counts were determined using the subread-1.5.0 function featureCounts, and counts were normalized to counts per million. To determine orthologous genes across species, whole genome alignments between GRCh38 and either the current primate references (panTro4, gorGor4, ponAbe2, rheMac8) or the updated great ape references panTro6 (Kronenberg et al, 2018) were generated using progressiveCactus (Paten et al., 2011). Outgroup genomes were gibbon (nomLeu3), bushbaby (otoGar3), squirrel monkey (saiBol1) and mouse (mm10). These alignments were

then used as input to CAT, using the GENCODE V27 annotation of GRCh38 as the annotation input. Species-specific RNA-seq and IsoSeq were used to help guide the annotation process (Fiddes et al, 2018). For this study, the resulting annotations on rheMac8 and the updated chimpanzee (panTro6) were used. CAT automatically defines orthology relationships using the information inherent in the whole genome alignment as well as subsequent filtering. This allows for quantification to be performed on the native species genome for a given experiment, and the resulting gene counts can be compared across species by their unique gene identifiers. In total, 49,360 genes annotated in human were identified in both chimpanzee and rhesus.

**De-multiplexing chimeric organoids—**To identify the species of origin for each cell from RNA-seq data, we compiled a list of diagnostic loci where the chimpanzee and human genome assemblies differ by a single-base substitution mutation that shows no sign of being polymorphic. We then analyze the RNA-seq reads from each cell at these genomic loci and calculate the number of times that we observe the human or chimp base. We created the diagnostic SNPs by examining whole-genome alignments of human (hg19) against chimpanzee (panTro4), gorilla (gorGor3), orangutan (ponAbe2), and rhesus (rheMac3) (Casper et al., 2018). To conservatively filter for syntenic alignments, we removed alignments involving segments that have not been placed on chromosomes or that represent alternative haplotypes as well as mandating similarity scores of at least 10000 (Kent et al., 2003). With the remaining set of high quality alignments, we located positions in the human genome where chimpanzee had a different base from human and there was no current data to suggest the position was polymorphic in dbSnp (Sherry et al., 2001). To guard against highly variable sites or alignment ambiguity, we ensured that at least one outgroup species (gorilla, orangutan, and rhesus) was present and the outgroup species agreed with either chimpanzee or human. This resulted in approximately 15 million diagnostic positions. For each single-cell RNA-seq library we mapped the reads to the human genome and analyzed the reads that overlapped a diagnostic position. In total, three organoids were initially seeded as chimeric in a pilot common garden experiment, but resulted in nearly pure outcomes for one species: H1.C7B.2 had 30/33 human cells, C1.1 had 39/49 chimpanzee cells, and C1.7 had 47/47 chimpanzee cells. As such, these organoids are displayed in Figure 1 and S1 heatmaps by the dominant species. The software used in this analysis is freely available under a BSD-style license (http://www.github.com/craiglowe).

**Clustering and Determining homologous cell types—**Datasets underwent quality control individually, removing any cells with fewer than 1000 genes/cell, greater than 20% of reads towards mitochondrial genes, and greater than 10% of ribosomal genes. Each dataset was then normalized and scaled. Clustering of individual datasets was performed as previously described (Lefebvre, 2008); (Shekhar et al., 2016); (Nowakowski et al., 2017) using a Jaccard weighted nearest neighbor distance in the space of significant principle components followed by Louvain clustering. Homologous cell types were generated using canonical correlation analysis (CCA) (Butler et al., 2018). CCA was performed in the space of 20 correlated dimensions, and tSNE was run in the space of the CCA dimensionality reduction for visualization. Clustering of combined datasets was then performed using the Louvain-Jaccard method in the space of CCA dimensions. We also developed an alternative

approach to co-cluster cells across model system or species that involved minimal transformation using a restricted set of marker genes for analysis. We first performed Louvain clustering using Jaccard distance on each dataset separately, as described above. We next selected the top 40 positive markers for each cluster from each dataset based on average difference. We then used a general linear model to remove markers with a high variance explained (typically greater than 0.1% to 1%) by model system or species, modeling these parameters as fixed effects. We then performed clustering of the combined dataset, scaled and normalized together, in the space of these restricted marker genes. This approach did not fully remove batch effects, but also retained cell subtype nuances from the original clustering and provided an independent validation of cell types as determined by CCA. Visualizations were performed in either tSNE space or using violin plots that reflected the $\log_2$(counts per million) value of gene expression.

**Determining co-expression modules—**WGCNA was performed using the top 2000–5000 PCA loading genes ranked across significant PCs based on absolute value of rotation scores using the WGCNA R package (Langfelder & Horvath, 2008). Parameters such as softPower, deepSplit, and cuttreeDynamic were determined independently for each dataset. To identify homologous modules from independent datasets, we used gene coexpression module kME scores across all genes to correlate modules derived from different datasets. Gene network maps presented are based on Pearson's correlation of expression levels of genes from each module, as specified in each figure legend.

**Differential expression and enrichment analysis—**Correlation analysis of networks to cell, species or protocol identity was performed by binarization of the variable of interest and using a Pearson's correlation to quantify the similarity across the dataset. When a correlation was performed across two cell types or other defined variables across the axis, only this set of cells was used, otherwise the whole dataset was utilized. Differential expression analysis at the gene level was performed using the likelihood ratio test and with a binary distribution suited to zero inflated data. In order to be considered as a differentially expressed gene, the average fold change was required to exceed an absolute value of $\log_2(0.25)$ and the frequency of expression was required to be greater than 25% across cells in at least one dataset. For determining genes differentially expressed during cortical development, we focused just on FOXG1+ organoids when focusing on telencephalic cell types. For each pairwise comparison, we used a general linear mixed model through the variance partition package (G. E. Hoffman & Schadt, 2016) to evaluate the extent to which fixed effects of cell type, donor, and species or protocol explain variation in each co-expression network. In all three pairwise comparisons, the majority of networks that could be explained by these factors related to cell type, with donorID, protocol, and species, explaining substantial variation in a smaller set of co-expression modules. Enrichment analysis for module signaling pathways was performed by intersecting gene lists with curated pathways in Enrichr (Chen et al., 2013). Adjusted p-values from this analysis are represented by $-\log_{10}$(p-value) in histograms.

**Western blots—**Protein was isolated using modified RIPA buffer (Millipore Sigma) with protease inhibitor cocktail (Millipore Sigma) and PhosStop phosphate inhibitor (Millipore

Sigma). Dissociated pellets of human or macaque cells, or week 5 organoids were resuspended in RIPA and vortexed. The lysate was incubated on ice for 30 minutes, after which lysates were spun for 10 minutes at 10,000 × g to eliminate debris. The supernatant protein was quantified using Pierce BCA Protein Assay Kit (Thermo Scientific). 50 ug of primary cell protein and 25 ug of organoid protein was loaded with 4× LDS loading dye plus 10% β-mercaptoethanol on a gradient 4 – 15 % gel (Mini Protean TGX, BioRad) in MOPS SDS buffer (Thermo Scientific). Wet transfers were performed with transfer buffer (Thermo Scientific) with 20% methanol. Blocking and antibody incubation was perfomed in Odyssey Blocking Buffer (Licor). Washes were performed with PBS plus 0.1% Tween-20. Primary antibodies (pS6 [Cell Signaling Technology; 2211], pNRDG1 [Cell Signaling Technology, 5482], p4EBP1 [Cell Signaling Technology, 2855], INSR [Novus, NBP2–12793], β-tubulin [Millipore Sigma, A1978], all 1:1000) were incubated overnight a 4° C, and secondary antibodies were inc ubated for 45 minutes at room temperature. Species specific IgG LT antibodies (Licor) were used at 1:10000. IRDye 680 or 800 secondary antibodies were used. Scanning was perfomed using the Licor Odyssey software and quantification was performed using Image Studio Lite, signal/area for each band. This signal was normalized to β-tubulin for each comparison and fold changes were calculated for each pair of samples run on the same blot (n= 3 for each species, for each primary and organoid comparisons). All antibodies were verified to bind to conserved epitopes between species.

### QUANTIFICATION AND STATISTICAL ANALYSIS

Quantification of images was performed using the Imaris Image Analysis software (Bitplane). Western blot quantification was performed using the Image Studio analysis suite (Licor). Statistical analysis was performed using either Microsoft Excel or Prism (GraphPad). Statistical tests, significance values, and experimental n are included in figure legends.

### DATA AND SOFTWARE AVAILABILITY

The sequencing data have been deposited in GEO under ID code GEO: GSE124299 and dbGaP phs000989.v3.

## Supplementary Material

Refer to Web version on PubMed Central for supplementary material.

## ACKNOWLEDGMENTS

The authors thank Y. Gilad, T. MacKenzie, S. Mokhtari, A. Tarantal, A. Fox, S. Wang, L. Adame, C. Villarreal, G. Wang, M. Snyder, T. Wang, D. Gordon, D. Kingsley and members of A.R.K and A.A.P labs for helpful discussion, reagents, and samples. This study was supported by CIRM (GC1R-06673-C to A.R.K.), Damon Runyon Foundation (DRG-2166–13 to A.A.P.), NIH (U01 MH105989 to A.R.K, F32 NS103266–02 to A.B.), Simons Foundation (SFARI 491371 to TJN) the Bowes Foundation, and ORIP/OD P51OD011132. RNA sequencing data has been deposited to GSE124299 and phs000989.v3.

## REFERENCES


Bakken TE, Miller JA, Ding S-L, Sunkin SM, Smith KA, Ng L, Szafer A, Dalley RA, Royall JJ, Lemon T, et al. (2016). A comprehensive transcriptional map of primate brain development. Nature 535, 367–375. [PubMed: 27409810]

Bershteyn M, Nowakowski TJ, Pollen AA, Di Lullo E, Nene A, Wynshaw-Boris A, and Kriegstein AR (2017). Human iPSC-Derived Cerebral Organoids Model Cellular Features of Lissencephaly and Reveal Prolonged Mitosis of Outer Radial Glia. Cell Stem Cell 20, 435–449.e4. [PubMed: 28111201]

Blake LE, Thomas SM, Blischak JD, Hsiao CJ, Chavarria C, Myrthil M, Gilad Y, and Pavlovic BJ (2018). A comparative study of endoderm differentiation in humans and chimpanzees. Genome Biology 19, 162. [PubMed: 30322406]

Boyd JL, Skove SL, Rouanet JP, Pilaz L-J, Bepler T, Gordân R, Wray GA, and Silver DL (2015). Human-chimpanzee differences in a FZD8 enhancer alter cell-cycle dynamics in the developing neocortex. Current Biology 25, 772–779. [PubMed: 25702574]

Butler A, Hoffman P, Smibert P, Papalexi E, and Satija R (2018). Integrating single-cell transcriptomic data across different conditions, technologies, and species. Nat. Biotechnol 48, 1070.

Camp JG, Badsha F, Florio M, Kanton S, Gerber T, Wilsch-Bräuninger M, Lewitus E, Sykes A, Hevers W, Lancaster M, et al. (2015). Human cerebral organoids recapitulate gene expression programs of fetal neocortex development. PNAS 112, 15672–15677. [PubMed: 26644564]

Ceccarelli M, Barthel FP, Malta TM, Sabedot TS, Salama SR, Murray BA, Morozova O, Newton Y, Radenbaugh A, Pagnotta SM, et al. (2016). Molecular Profiling Reveals Biologically Discrete Subsets and Pathways of Progression in Diffuse Glioma. Cell 164, 550–563. [PubMed: 26824661]

Charrier C, Joshi K, Coutinho-Budd J, Kim J-E, Lambert N, de Marchena J, Jin W-L, Vanderhaeghen P, Ghosh A, Sassa T, et al. (2012). Inhibition of SRGAP2 Function by Its Human-Specific Paralogs Induces Neoteny during Spine Maturation. Cell 149, 923–935. [PubMed: 22559944]

Chen EY, Tan CM, Kou Y, Duan Q, Wang Z, Meirelles GV, Clark NR, and Ma'ayan A (2013). Enrichr: interactive and collaborative HTML5 gene list enrichment analysis tool. BMC Bioinformatics 14, 128. [PubMed: 23586463]

Clevers H (2016). Modeling Development and Disease with Organoids. Cell 165, 1586–1597. [PubMed: 27315476]

Dennis MY, Harshman L, Nelson BJ, Penn O, Cantsilieris S, Huddleston J, Antonacci F, Penewit K, Denman L, Raja A, et al. (2017). The evolution and population diversity of human-specific segmental duplications. Nat Ecol Evol 1, 69. [PubMed: 28580430]

Dennis MY, Nuttle X, Sudmant PH, Antonacci F, Graves TA, Nefedov M, Rosenfeld JA, Sajjadian S, Malig M, Kotkiewicz H, et al. (2012). Evolution of Human-Specific Neural SRGAP2 Genes by Incomplete Segmental Duplication. Cell 149, 912–922. [PubMed: 22559943]

Eiraku M, Takata N, Ishibashi H, Kawada M, Sakakura E, Okuda S, Sekiguchi K, Adachi T, and Sasai Y (2011). Self-organizing optic-cup morphogenesis in three-dimensional culture. Nature 472, 51–56. [PubMed: 21475194]

Eiraku M, Watanabe K, Matsuo-Takasaki M, Kawada M, Yonemura S, Matsumura M, Wataya T, Nishiyama A, Muguruma K, and Sasai Y (2008). Self-organized formation of polarized cortical tissues from ESCs and its active manipulation by extrinsic signals. Cell Stem Cell 3, 519–532. [PubMed: 18983967]

Fish JL, Dehay C, Kennedy H, and Huttner WB (2008). Making bigger brains-the evolution of neural-progenitor-cell division. J. Cell. Sci 121, 2783–2793. [PubMed: 18716282]

Florio M, Namba T, Pääbo S, Hiller M, and Huttner WB (2016). A single splice site mutation in human-specific ARHGAP11B causes basal progenitor amplification. Sci Adv 2, e1601941–e1601941. [PubMed: 27957544]

Gallego Romero I, Pavlovic BJ, Hernando-Herraez I, Zhou X, Ward MC, Banovich NE, Kagan CL, Burnett JE, Huang CH, Mitrano A, et al. (2015). A panel of induced pluripotent stem cells from chimpanzees: a resource for comparative functional genomics. Elife 4, e07103. [PubMed: 26102527]

Herculano-Houzel S (2012). The remarkable, yet not extraordinary, human brain as a scaled-up primate brain and its associated cost. PNAS 109 Suppl 1, 10661–10668. [PubMed: 22723358]

Hoffman GE, and Schadt EE (2016). variancePartition: interpreting drivers of variation in complex gene expression studies. BMC Bioinformatics 17, 483. [PubMed: 27884101]

Johnson ME, Viggiano L, Bailey JA, Abdul-Rauf M, Goodwin G, Rocchi M, and Eichler EE (2001). Positive selection of a gene family during the emergence of humans and African apes. Nature 413, 514–519. [PubMed: 11586358]

Kadoshima T, Sakaguchi H, Nakano T, Soen M, Ando S, Eiraku M, and Sasai Y (2013). Self-organization of axial polarity, inside-out layer pattern, and species-specific progenitor dynamics in human ES cell-derived neocortex. Proc Natl Acad Sci U S A 110, 20284–20289. [PubMed: 24277810]

Kriegstein A, Noctor S, and Martínez-Cerdeño V (2006). Patterns of neural stem and progenitor cell division may underlie evolutionary cortical expansion. Nat Rev Neurosci 7, 883–890. [PubMed: 17033683]

Lancaster MA, Renner M, Martin C-A, Wenzel D, Bicknell LS, Hurles ME, Homfray T, Penninger JM, Jackson AP, and Knoblich JA (2013). Cerebral organoids model human brain development and microcephaly. Nature 501, 373–379. [PubMed: 23995685]

Langfelder P, and Horvath S (2008). WGCNA: an R package for weighted correlation network analysis. BMC Bioinformatics 9, 559. [PubMed: 19114008]

Lefebvre V (2008). Fast unfolding of communities in large networks. Journal of Statistical Mechanics: Theory and Experiment 2008, P10008.

Marchetto MCN, Narvaiza I, Denli AM, Benner C, Lazzarini TA, Nathanson JL, Paquola ACM, Desai KN, Herai RH, Weitzman MD, et al. (2013). Differential L1 regulation in pluripotent stem cells of humans and apes. Nature 503, 525–529. [PubMed: 24153179]

McLean CY, Reno PL, Pollen AA, Bassan AI, Capellini TD, Guenther C, Indjeian VB, Lim X, Menke DB, Schaar BT, et al. (2011). Human-specific loss of regulatory DNA and the evolution of human-specific traits. Nature 471, 216–219. [PubMed: 21390129]

Mora-Bermúdez F, Badsha F, Kanton S, Camp JG, Vernot B, Köhler K, Voigt B, Okita K, Maricic T, He Z, et al. (2016). Differences and similarities between human and chimpanzee neural progenitors during cerebral cortex development. Elife 5, 166.

Noctor SC, Flint AC, Weissman TA, Dammerman RS, and Kriegstein AR (2001). Neurons derived from radial glial cells establish radial units in neocortex. Nature 409, 714–720. [PubMed: 11217860]

Nowakowski TJ, Bhaduri A, Pollen AA, Alvarado B, Mostajo-Radji MA, Di Lullo E, Haeussler M, Sandoval-Espinosa C, Liu SJ, Velmeshev D, et al. (2017). Spatiotemporal gene expression trajectories reveal developmental hierarchies of the human cortex. Science 358, 1318–1323. [PubMed: 29217575]

Ohno S (1970). Evolution by Gene Duplication (Berlin, Heidelberg: Springer Berlin Heidelberg).

Oldham MC, Konopka G, Iwamoto K, Langfelder P, Kato T, Horvath S, and Geschwind DH (2008). Functional organization of the transcriptome in human brain. Nature 11, 1271–1282.

Onorati M, Li Z, Liu F, Sousa AMM, Nakagawa N, Li M, Dell'Anno MT, Gulden FO, Pochareddy S, Tebbenkamp ATN, et al. (2016). Zika Virus Disrupts Phospho-TBK1 Localization and Mitosis in Human Neuroepithelial Stem Cells and Radial Glia. Cell Rep 16, 2576–2592. [PubMed: 27568284]

Otani T, Marchetto MC, Gage FH, Simons BD, and Livesey FJ (2016). 2D and 3D Stem Cell Models of Primate Cortical Development Identify Species-Specific Differences in Progenitor Behavior Contributing to Brain Size. Cell Stem Cell 18, 467–480. [PubMed: 27049876]

Parikshak NN, Luo R, Zhang A, Won H, Lowe JK, Chandran V, Horvath S, and Geschwind DH (2013). Integrative functional genomic analyses implicate specific molecular pathways and circuits in autism. Cell 155, 1008–1021. [PubMed: 24267887]

Paten B, Earl D, Nguyen N, Diekhans M, Zerbino D, and Haussler D (2011). Cactus: Algorithms for genome multiple sequence alignment. Genome Research 21, 1512–1528. [PubMed: 21665927]

Pavlovic BJ, Blake LE, Roux J, Chavarria C, and Gilad Y (2018). A Comparative Assessment of Human and Chimpanzee iPSC-derived Cardiomyocytes with Primary Heart Tissues. Sci Rep 8, 15312. [PubMed: 30333510]

Peng N, Meng N, Wang S, Zhao F, Zhao J, Su L, Zhang S, Zhang Y, Zhao B, and Miao J (2014). An activator of mTOR inhibits oxLDL-induced autophagy and apoptosis in vascular endothelial cells and restricts atherosclerosis in apolipoprotein EË/Ë mice. Sci Rep 4, 5519.

Poduri A, Evrony GD, Cai X, Elhosary PC, Beroukhim R, Lehtinen MK, Hills LB, Heinzen EL, Hill A, Hill RS, et al. (2012). Somatic activation of AKT3 causes hemispheric developmental brain malformations. Neuron 74, 41–48. [PubMed: 22500628]

Pollard KS, Salama SR, Lambert N, Lambot M-A, Coppens S, Pedersen JS, Katzman S, King B, Onodera C, Siepel A, et al. (2006). An RNA gene expressed during cortical development evolved rapidly in humans. Nature 443, 167–172. [PubMed: 16915236]

Pollen AA, Nowakowski TJ, Chen J, Retallack H, Sandoval-Espinosa C, Nicholas CR, Shuga J, Liu SJ, Oldham MC, Diaz A, et al. (2015). Molecular identity of human outer radial glia during cortical development. Cell 163, 55–67. [PubMed: 26406371]

Pollen AA, Nowakowski TJ, Shuga J, Wang X, Leyrat AA, Lui JH, Li N, Szpankowski L, Fowler B, Chen P, et al. (2014). Low-coverage single-cell mRNA sequencing reveals cellular heterogeneity and activated signaling pathways in developing cerebral cortex. Nat. Biotechnol 32, 1053–1058. [PubMed: 25086649]

Prescott SL, Srinivasan R, Marchetto MC, Grishina I, Narvaiza I, Selleri L, Gage FH, Swigut T, and Wysocka J (2015). Enhancer divergence and cis-regulatory evolution in the human and chimp neural crest. Cell 163, 68–83. [PubMed: 26365491]

Quadrato G, Nguyen T, Macosko EZ, Sherwood JL, Min Yang S, Berger DR, Maria N, Scholvin J, Goldman M, Kinney JP, et al. (2017). Cell diversity and network dynamics in photosensitive human brain organoids. Nature 545, 48–53. [PubMed: 28445462]

Rafalski VA, and Brunet A (2011). Energy metabolism in adult neural stem cell fate. Prog. Neurobiol 93, 182–203. [PubMed: 21056618]

Rakic P (1995). A small step for the cell, a giant leap for mankind: a hypothesis of neocortical expansion during evolution. Trends Neurosci 18, 383–388. [PubMed: 7482803]

Rakic P (2003). Developmental and evolutionary adaptations of cortical radial glia. Cerebral Cortex 13, 541–549.

Sakai T, Hirata S, Fuwa K, Sugama K, Kusunoki K, Makishima H, Eguchi T, Yamada S, Ogihara N, and Takeshita H (2012). Fetal brain development in chimpanzees versus humans. Current Biology 22, R791–R792. [PubMed: 23017988]

Shekhar K, Lapan SW, Whitney IE, Tran NM, Macosko EZ, Kowalczyk M, Adiconis X, Levin JZ, Nemesh J, Goldman M, et al. (2016). Comprehensive Classification of Retinal Bipolar Neurons by Single-Cell Transcriptomics. Cell 166, 1308–1323.e1330. [PubMed: 27565351]

Silver DL (2016). Genomic divergence and brain evolution: How regulatory DNA influences development of the cerebral cortex. Bioessays 38, 162–171. [PubMed: 26642006]

Sloan SA, Darmanis S, Huber N, Khan TA, Birey F, Caneda C, Reimer R, Quake SR, Barres BA, and Paúca SP (2017). Human Astrocyte Maturation Captured in 3D Cerebral Cortical Spheroids Derived from Pluripotent Stem Cells. Neuron 95, 779–790.e6. [PubMed: 28817799]

Smart IHMI, Dehay CC, Giroud PP, Berland MM, and Kennedy HH (2002). Unique morphological features of the proliferative zones and postmitotic compartments of the neural epithelium giving rise to striate and extrastriate cortex in the monkey. Cerebral Cortex 12, 37–53. [PubMed: 11734531]

Stessman HAF, Xiong B, Coe BP, Wang T, Hoekzema K, Fenckova M, Kvarnung M, Gerdts J, Trinh S, Cosemans N, et al. (2017). Targeted sequencing identifies 91 neurodevelopmental-disorder risk genes with autism and developmental-disability biases. Nat Genet 49, 515–526. [PubMed: 28191889]

Sudmant PH, Kitzman JO, Antonacci F, Alkan C, Malig M, Tsalenko A, Sampas N, Bruhn L, Shendure J, 1000 Genomes Project, et al. (2010). Diversity of Human Copy Number Variation and Multicopy Genes. Science 330, 641–646. [PubMed: 21030649]

Sudmant PH, Huddleston J, Catacchio CR, Malig M, Hillier LW, Baker C, Mohajeri K, Kondova I, Bontrop RE, Persengiev S, et al. (2013). Evolution and diversity of copy number variation in the great ape lineage. Genome Research 23, 1373–1382. [PubMed: 23825009]

Zhou J, Su P, Wang L, Chen J, Zimmermann M, Genbacev O, Afonja O, Horne MC, Tanaka T, Duan E, et al. (2009). mTOR supports long-term self-renewal and suppresses mesoderm and endoderm activities of human embryonic stem cells. PNAS 106, 7840–7845. [PubMed: 19416884]

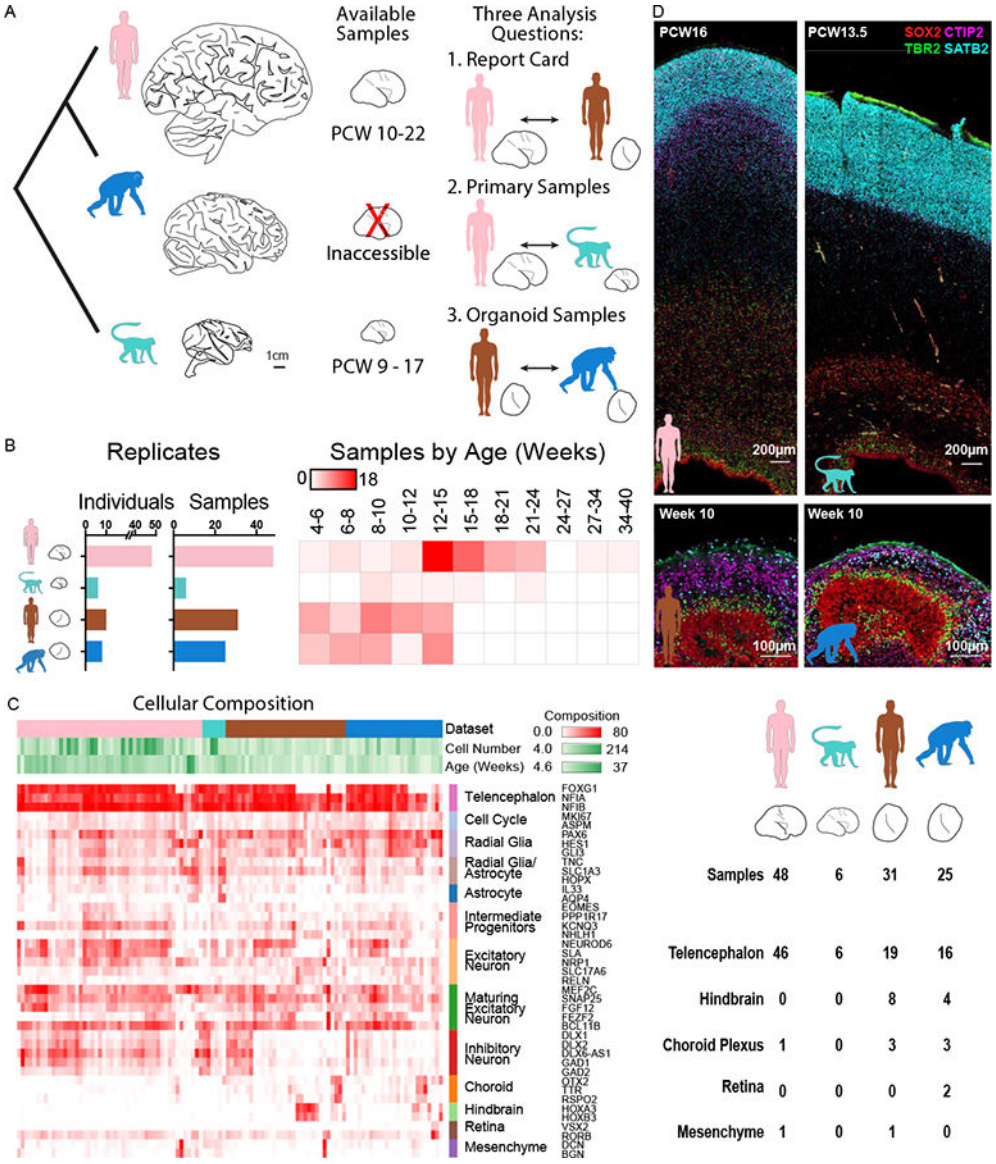


**Figure 1. Organoid models reflect normal features of human and chimpanzee brain development.**

**a)** The human brain has expanded dramatically compared with other primates, but brain tissue is largely inaccessible from developing chimpanzee. To compare human and chimpanzee development, our study focuses on three analysis questions that integrate data from primary human (pink) and macaque samples (light blue) with human (brown) and chimpanzee (blue) organoid models. **b)** Histograms and heatmap depict the number of individuals and primary or organoid samples and the distribution of samples over post conception or post differentiation weeks. **c)** Heatmap represents the fraction of cells expressing each marker gene across cells from each primary sample or organoid, and table summarizes the number of samples that predominantly express markers for a given regional identity. **d)** Immunohistochemistry for markers of radial glia (SOX2), intermediate progenitors TBR2 (EOMES), and neurons CTIP2 (BCL11B), SATB2, reveals histological and cellular features of normal neurogenesis in the germinal zones of human and

chimpanzee cerebral organoids, but a much more extensive intermediate zone and cortical plate in primary samples.

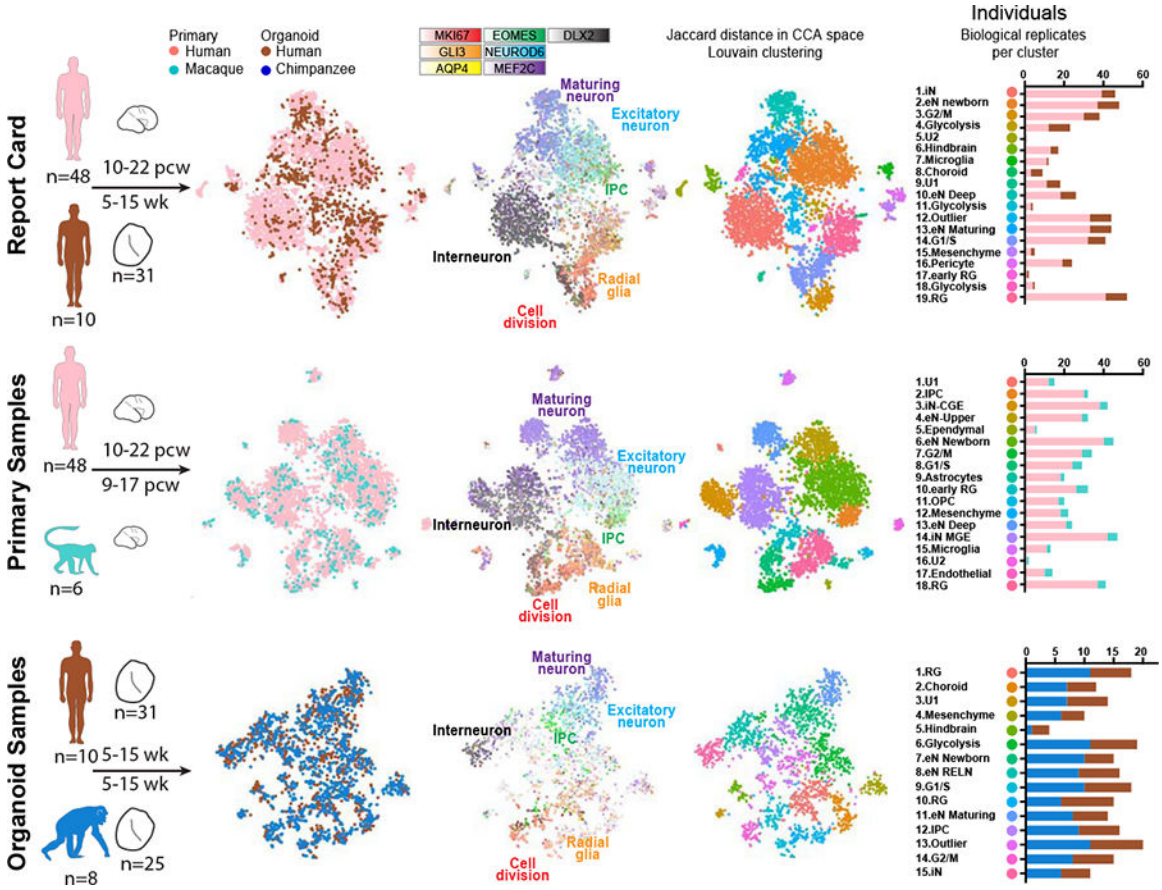


**Figure 2. Identification of homologous cell types across species and model system.**

**a-c)** Pairwise comparisons of human primary and human organoid cells (**a**), human primary and macaque primary cells (**b**), and human organoid and chimpanzee organoid cells (**c**), with developmental stages and the number of distinct individuals and organoids depicted under the schematics. Columns 1–3 display cells plotted based on gene expression similarity after principle components analysis and t-stochastic neighbor embedding, and colored by species or model system (column 1), by marker genes for known cell types (column 2), and by clusters following Louvain-Jaccard clustering (column 3). Column 4 indicates the number of primary individuals or distinct iPS lines contributing to each cluster.

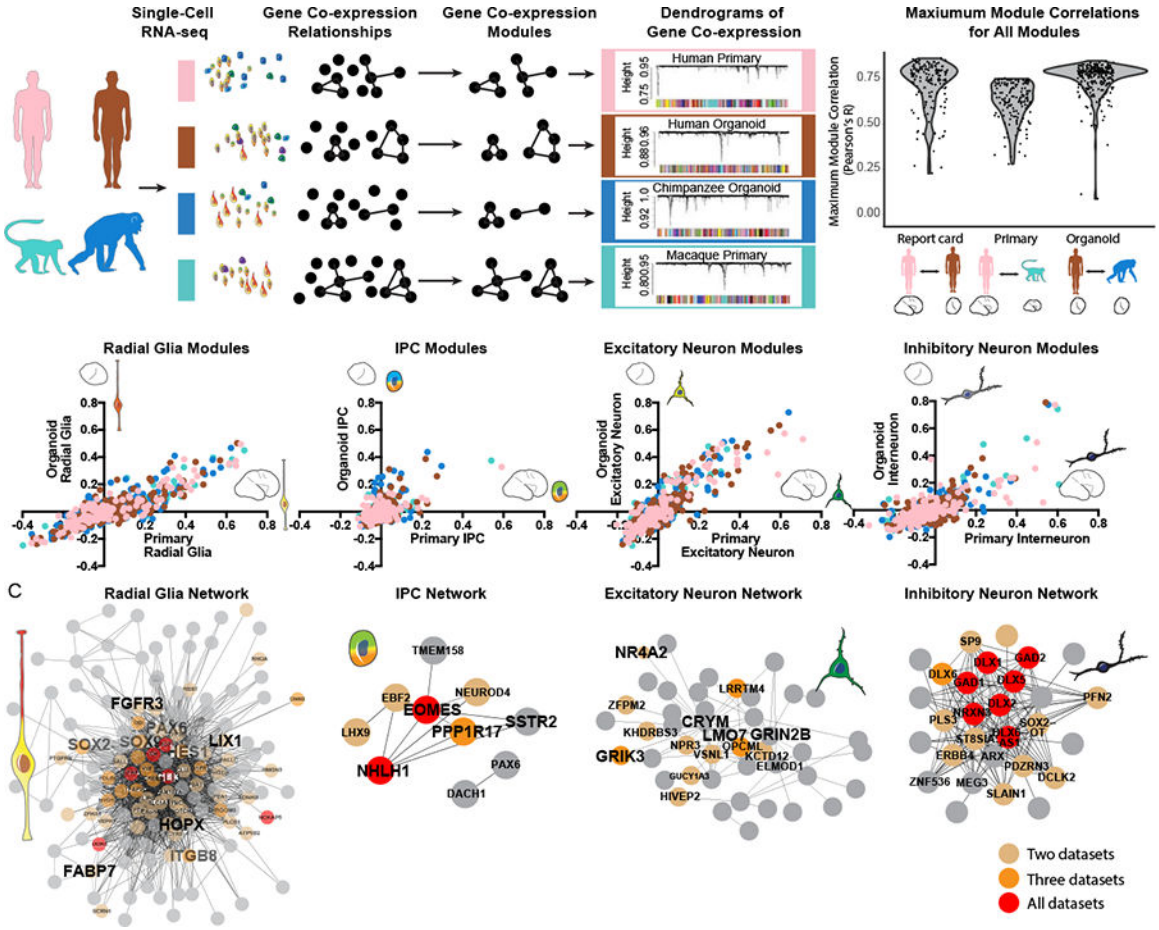


**Figure 3. Conservation of gene co-expression modules across species and model system.**

**a)** Gene co-expression relationships were determined independently in each dataset using WGCNA. Violin plots indicate the distribution of maximum correlation values for all co-expression modules in each pairwise comparison. **b)** Scatterplots depict the correlation of modules to cell types independently determined in organoid (Y-axis) and primary cell datasets (X-axis). Notably many modules correlate to coarse cell-type classifications, representing finer cell subtypes and states. Dots are colored by the model system in which the network was identified. **c)** Network maps depict the correlation of genes from top cell type networks across all four datasets. Edges represent a correlation with $R > 0.25$, with edge length inversely related to correlation strength. Brown, orange and red dots highlight genes that appear in the core module for 2, 3 and 4 networks respectively.

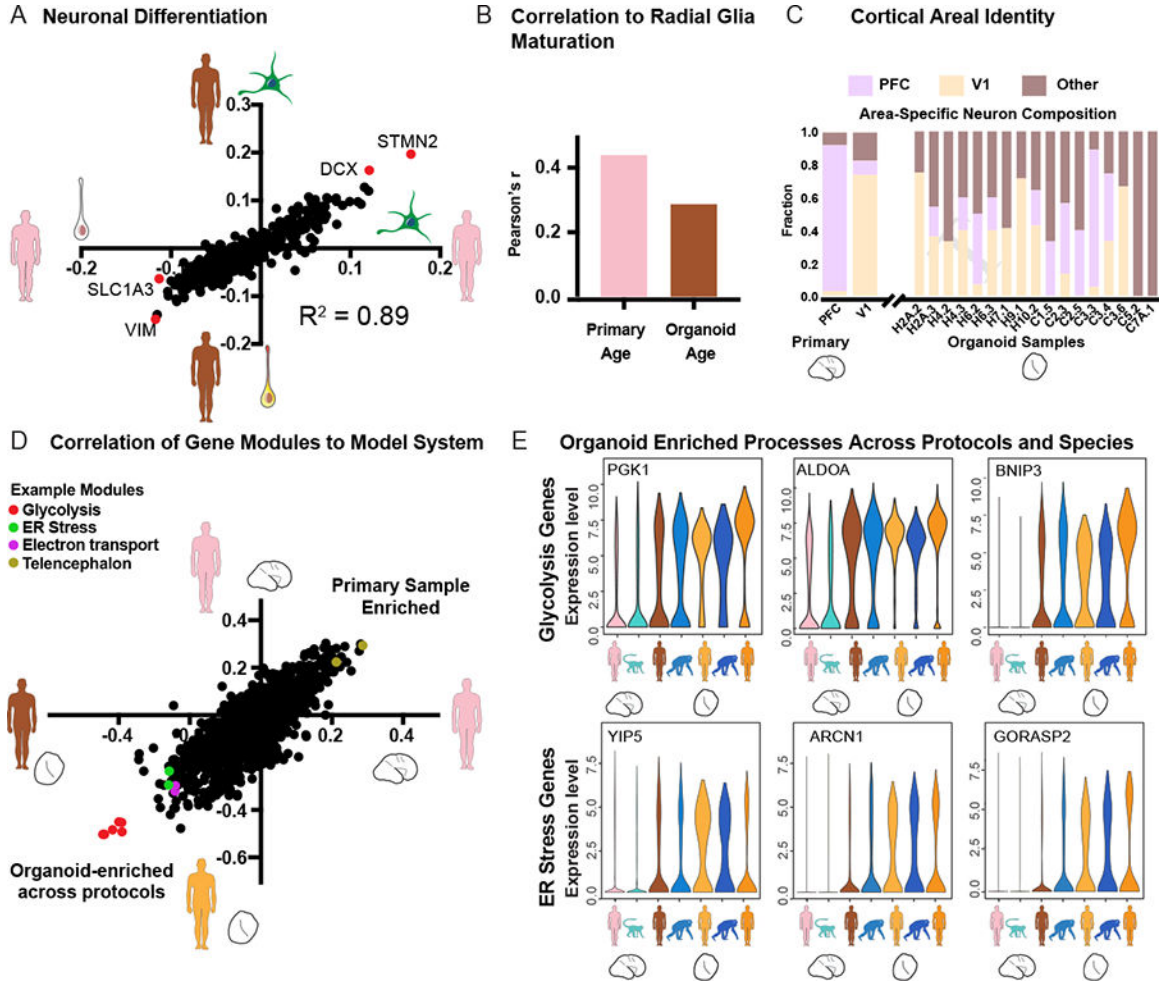


**Figure 4. Organoid modules recapitulate developmental gene expression trajectories but exhibit elevated metabolic stress across protocols.**

**a)** Scatterplot shows the correlation of genes to the neuronal differentiation signature as derived in organoids (Y-axis) and in primary cells (X-axis). **b)** Histogram of R values indicating the correlation of the radial glia maturation network to sample age across primary radial glia (PCW8–22) and organoid radial glia (Week 5–15). **c)** Areal identity of maturing excitatory neurons in primary tissue and across organoids as predicted by a classifier. First two columns indicate primary cells with known areal identity. **d)** Scatterplot shows the correlation of all gene co-expression modules to primary human cells (positive on both axes) versus organoid cells from this paper using the Kadoshima protocol (negative on X-axis) and a previous paper (Camp et al., 2015) using a whole brain organoid protocol (negative on Y-axis). Modules are generated independently in each dataset and correlated to primary or organoid cell identity. Glycolysis, endoplasmic-reticulum (ER) stress, and electron transport modules show a strong correlation with organoid cells from both protocols. **e)** Violin plots illustrate the distribution of single cell gene expression values for hub genes in the glycolysis and ER stress co-expression modules from primary human and macaque cells (columns 1 and 2) organoid cells generated in this paper using the Kadoshima protocol (columns 3 and 4), organoid cells generated using a whole brain organoid protocol (columns 5 and 6, Camp

et al., 2015; Mora-Bermudez et al., 2016) and a cortical spheroid protocol (column 7, Sloan et al., 2017).

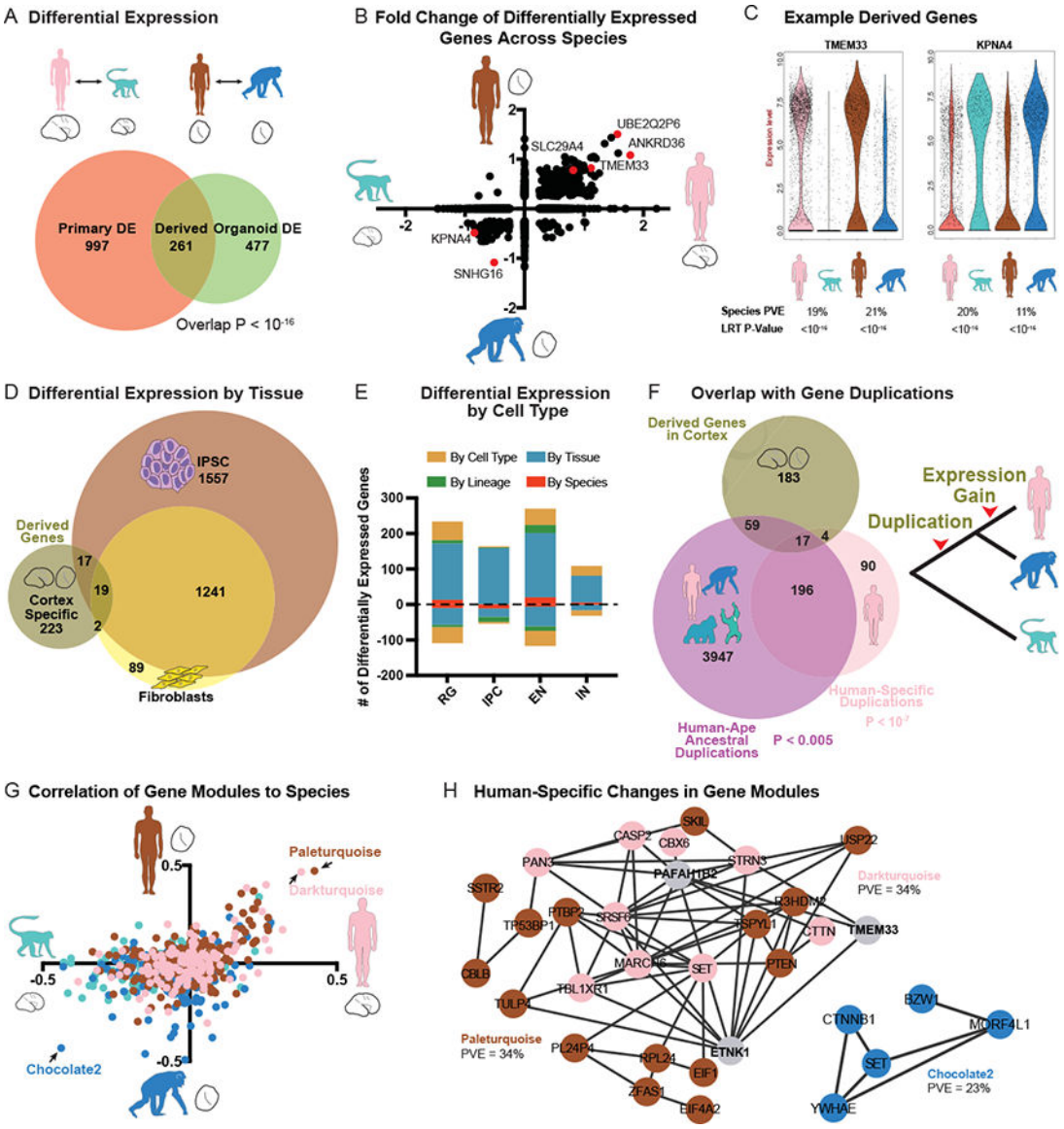


**Figure 5. Human-specific gene expression patterns during cortical neurogenesis.**

**a)** Venn diagram represents the number of differentially expressed genes between primary human and macaque (left circle) and differentially expressed genes between human and chimpanzee organoids with cortical identity (LRT adjusted p-value < 0.0005). Overlap represents candidate genes with human-specific regulatory changes. **b)** Scatterplot illustrates the fold change for genes differentially expressed in either primary cell or organoid cell comparisons across all cells. **c)** Violin plots for genes up- or down-regulated specifically in human cells. **d)** Venn diagram represents the overlap between derived regulatory changes in cortex and human and chimpanzee differential expression previously determined in fibroblasts and iPS cells (Gallego Romero et al., 2015). **e)** Histogram highlights the number of derived expression changes that are shared across cortex, iPSC, and fibroblasts (by species, red), found only in cortex (by tissue, blue), found only in the excitatory neuron lineage of radial glia, intermediate progenitor cells (IPC) and excitatory neurons (by lineage,

green), or in one cortical cell type (by cell type, dark yellow). **f)** Venn diagram represents the overlap between derived genes in cortex, and genes with duplications or copy number expansions that are human-specific (pink) or occurred in apes along the lineage leading to humans, prior to our divergence with chimpanzee (purple) (Sudmant et al., 2013). Note that some genes underwent multiple duplication events along the human lineage (overlap between pink and purple circles). **g)** Scatterplot illustrates the correlation of each gene co-expression module to species across primary cells (X-axis) and organoid cells (Y-axis). Colors correspond to the dataset in which the module was generated. **h)** Network maps highlight genes from the modules with expression most correlated to human or primate cell sources. Edges correspond to a correlation $R > 0.25$.

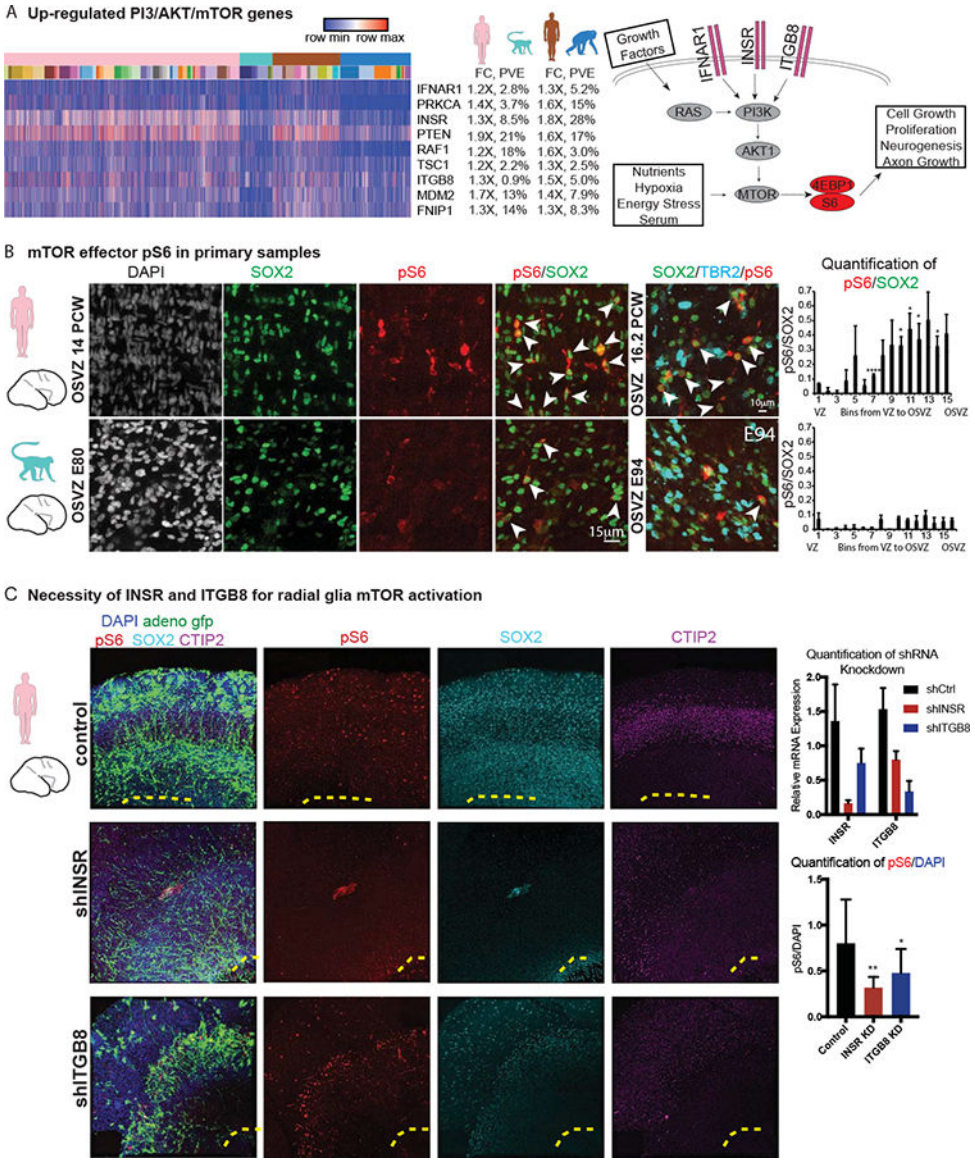


**Figure 6. Human outer subventricular zone radial glia show increased phosphorylation of the mTOR effector S6 compared to other primates.**

**a)** Heatmap across all cells (columns) illustrating differential expression for a subset genes related to the PI3K/AKT/mTOR pathway, with label showing the $\log_2$(fold change) and percent variance explained by species in both the primary cell and the organoid cell comparison. Schematic highlights receptors upregulated in human and their relationship to downstream effectors, phosphorylated S6 (pS6) and phosphorylated 4EBP1 (p4EBP1). **b)** Immunohistochemistry illustrates abundant labeling of pS6 in radial glia of primary human outer subventricular zone compared to primary macaque. Quantification of the levels of pS6 is shown in equal bins across the ventricular and outer subventricular zone. * denotes significant up-regulation in human compared to macaque with p <0.05 (*) or p <- 0.0001 (****) in each bin, with aggregated across bins significant at $p < 10^{-6}$ (Welch's t-test). **c)** Immunohistochemistry in human slice culture (representative example, n = 4) shows the fiber architecture (adeno GFP), pS6, SOX2 (progenitor population), and CTIP2 (neuronal

population) in slices treated with hairpins targeting INSR or ITGB8. Quantification of knockdown and pS6 levels in outer subventricular zone is also shown. Note the control sample also contains pS6 in the cortical plate as previously observed. * indicates significant downregulation of pS6 levels with $p < 0.05$ (*) or $p < 0.01$ (**) (Welch's t-test).

**Table 1**

KEY RESOURCES TABLE

| REAGENT or RESOURCE | SOURCE | IDENTIFIER |
|---|---|---|
| Antibodies | | |
| anti-TBR2, sheep, 1:150 | R&D Systems | Cat# AF6166 |
| anti-pS6, rabbit, 1:100 | Cell Signaling | Cat# 2211S |
| anti-SOX2, goat, 1:200 | Santa Cruz Biotechnology | Cat# SC17320 |
| anti-SOX2, mouse, 1:200 | Santa Cruz Biotechnology | Cat# SC365964 |
| anti-TUJ1, mouse, 1:500 | Covance | Cat# MMS-435 |
| anti-PAX6, rabbit, 1:500 | Covance | Cat# PRB-278P |
| anti-CTIP2, rat, 1:500 | Abcam | Cat# ab18465 |
| anti-TBR1, rabbit, 1:500 | Abcam | Cat# ab31940 |
| anti-SATB2, rabbit, 1:1000 | Abcam | Cat# ab34735 |
| anti-GFP, goat, 1:500 | Abcam | Cat# ab5450 |
| anti-pNRDG1, rabbit, 1:1000 | Cell Signaling | Cat# 5482 |
| anti-p4EBP1, rabbit, 1:1000 | Cell Signaling | Cat# 2855 |
| anti-INSR, rabbit, 1:1000 | Novus Biologicals | Cat# NBP2–12793 |
| anti-β-tubulin, mouse, 1:1000 | Millipore Sigma | Cat# A1978 |
| | | |
| | | |
| | | |
| | | |
| | | |
| | | |
| | | |
| | | |
| | | |
| Bacterial and Virus Strains | | |
| CMV::GFP adenovirus | Vector Biolabs | Cat# 1060 |
| | | |
| | | |
| | | |
| | | |
| Biological Samples | | |
| | | |
| | | |
| | | |
| | | |
| | | |
| Chemicals, Peptides, and Recombinant Proteins | | |
| Rapamycin, 250 nM | Abcam | Cat# ab146591 |
| BDNF, 20ng/mL | Millipore Sigma | Cat# SRP3014–10 |
| 3-Benzyl-5-((2-nitrophenoxy)methyl)-dihydrofuran-2(3H)-one (3BDO) (Peng et al., 2014), 60uM | Millipore Sigma | Cat# SML1687 |
| Rock Inhibitor Y-27632 | Tocris | Cat# 1254 |
| IWR-1-endo | Cayman Chemical | Cat# 13659 |
| SB431542 | Tocris | Cat# 1614 |
| | | |
| Critical Commercial Assays | | |
| | | |
| | | |
| | | |

| REAGENT or RESOURCE | SOURCE | IDENTIFIER |
|---|---|---|
| | | |
| | | |
| Deposited Data | | |
| Raw and processed organoid and macaque data | This paper | GEO: GSE124299 |
| Raw and processed primary human data | Nowakowski et al., 2017 | dbGaP: phs000989.v3 |
| | | |
| | | |
| | | |
| Experimental Models: Cell Lines | | |
| C1-PR00738-male | This paper | RRID: CVCL_2X19 |
| C2-S003649-male | Gilad lab-Gallego Romero et al., 2015 | RRID: CVCL_1G31 |
| C3-S008861-male | Gilad lab-Gallego Romero et al., 2015 | RRID: CVCL_1G34 |
| C4–40290G-male | Gilad lab-Pavlovic et al., 2018 | |
| C5-S004955-male | Gilad lab-Gallego Romero et al., 2015 | RRID: CVCL_1G33 |
| C6–40210A-male | Gilad lab- Gallego Romero et al., 2015 | RRID: CVCL_1G35 |
| C7A-S003611-male | This paper | RRID: CVCL_V833 |
| C7B-S003611-male | This paper | RRID: CVCL_V833 |
| C8-PR00226-male | This paper | RRID: CVCL_2V65 |
| H1-CRL-2522-male | Hsiao lab-Matsumoto et al., 2013 | RRID: CVCL_3653 |
| H2A-1323.2-female | Hsiao lab-Matsumoto et al., 2013 | RRID: CVCL_0G83 |
| H2B-1323.4-female | Hsiao lab-Matsumoto et al., 2013 | RRID: CVCL_0G84 |
| H3-GM25256-male | Conklin lab-Kreitzer et al., 2013 | RRID: CVCL_Y803 |
| H4-IPSC.C-male | Bucay lab | |
| H5–28815-male | Gilad-26102527 | |
| H6–28126-male | Gilad-26102527 | |
| H7-CESCG-295-male | Wang lab-CESCG | |
| H8-H23555A-male | Gilad-26102527 | |
| H9-SSC-PB1-male | Wang lab -CESCG | |
| H10-CESCG-297-male | Wang lab -CESCG | |
| | | |
| | | |
| Experimental Models: Organisms/Strains | | |
| | | |
| | | |
| | | |
| | | |
| | | |
| | | |
| Oligonucleotides | | |
| SRCAP in situ probe sequence:<br>ATTTAGGTGACACTATAGCCGCCTACCCCAAGAGGAG<br>GAGGAGGGGCCAGGGGCTGGGGATGAGAGTTCCTG<br>TGGGACTGGTGGAGGCACCCACCGGCGCAGTAAAAA<br>GGCCAAGGCCCCTGAGAGGCCAGGGACTCGTGTCAG<br>TGAGCGTCTTCGTGGAGCCCGGGCTGAGACTCAAGG<br>GGCAAACCACACTCCTGTCATATCCGCCCATCAAACTC<br>GCAGCACCACCACACCGCCCCGCTGCAGTCCTGCCAG<br>GGAGAGAGTTTCCAGGCCAGCACCTAGGCCTCGACC<br>CACTCCAGCTTCAGCTCCAGCTGCAATTCCTGCCCTTG<br>TTCCTGTCCCAGTCTCTGCCCCAGTACCCATTTCAACC<br>CCAAATCCAATAACCATTCTCCCTGTCCATATATTGCC | IDT, this paper | N/A |

| REAGENT or RESOURCE | SOURCE | IDENTIFIER |
|---|---|---|
| TTCTCCCCCCCCTCCACAGATTCCTCCTTGTTCTCCTGC CTGCACCCCTCCTCCCGCCTGTACCCTATAGTGAGTCG TATTACTC | | |
| SLC29A4 in situ probe sequence: ATTTAGGTGACACTATAGTGGCAGCTCTGCCCGTGGA CTGGCGGGGCACCCACCTGCTGGCCTGCTCCTGCCTG CGCATAGTCTTCATCCCTCTCTTCATCCTGTGCGTCTAC CCCAGCGGCACGCCCGCCCTGCGCCACCCCGCCTGGC CCTGCATCTTCTCGCTGCTTATGGGCATCAGCAACGG CTACTTCGGCAGCGTGCCCATGATCCTGGCGGCGGGC AAAGTGAGCCCCAAGCAGCGGGAGCTGGCAGGGAA CACCATGACCGTGTCCTACATGTCGGGGCTGACACTG GGGTCCGCCGTGGCCTACTGCACCTACAGCCTCACCC GCGACGCCCACGGCAGCTGCCTGCACCCCTCCACCGC CAATGGCTCCATCCTCTCAGGCCTCTGAGCCAGCTCTG CCCACTGCCAGGGATGCCGAGGGCCTGACCAGGGGC CCCAAGGCCTGAAGGCCCCTCCCCCGTCCCCACCCTAT AGTGAGTCGTATTACTC | IDT, this paper | N/A |
| | | |
| | | |
| | | |
| Recombinant DNA | | |
| pCXLE-hOCT3/4-shp53-F (OCT3/4 and p53 shRNA) | Okita et al., 2011 | Addgene 27077 |
| pCXLE-hSK (SOX2, KLF4) | Okita et al., 2011 | Addgene 27078 |
| pCXLE-hUL (L-MYC, LIN28) | Okita et al., 2011 | Addgene 27080 |
| pCXLE-EGFP (negative control) | Okita et al., 2011 | Addgene 27082 |
| | | |
| Software and Algorithms | | |
| | | |
| | | |
| | | |
| | | |
| | | |
| Other | | |
| | | |
| | | |
| | | |
| | | |
| | | |